U. S. Geological Survey.

REPORTS-OPEN FILE SERIES, no. 77-93:

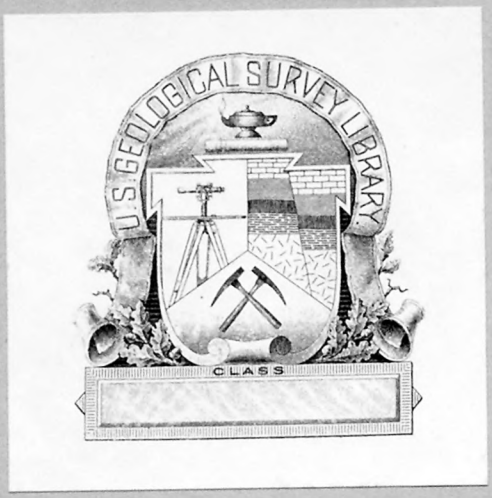
U.S. GEOLOGICAL SURVEY LIBRARY
CLASS

The Yellow Dog Peridotite and A Possible Buried Igneous Complex of Lower Keweenawan Age in The Northern Peninsula of Michigan

by

John S. Klasner[1/], David W. Snider[2/],

W. F. Cannon[1/], and John F. Slack[1/]

[1/] U. S. Geological Survey, Reston, Va.

[2/] Geological Survey Division, Michigan Dept. of Natural Resources, Lansing, Mich.

U. S. Geological Survey Open-file Report

U. S. Geological Survey
OPEN FILE REPORT 77-93
This report is preliminary and has not been edited or reviewed for conformity with Geological Survey standards or nomenclature.

U. S. GOVERNMENT PRINTING OFFICE : 1972 O - 457 089

Contents

U.S. GOVERNMENT PRINTING OFFICE: 1992 O - 454-864

Tables

U. S. GOVERNMENT PRINTING OFFICE : 1972 O - 457-864

Illustrations

U. S. GOVERNMENT PRINTING OFFICE : 1972 O - 455-109

Abstract

Partly serpentinized peridotite of early Keweenawan age crops out in two places along a 20-km-long zone of positive aeromagnetic anomalies in northern Marquette County, Michigan. Most of the area is mantled by Pleistocene drift and the bedrock is not exposed.

Petrographic and electron microprobe studies show that the peridotite was originally a plagioclase lherzolite containing 40-50% olivine (Fo_{80}) and approximately 10-15% each of enstatite($En_{78}Wo_{04}Fs_{18}$) and diopsidic augite ($En_{47}Wo_{42}Fs_{11}$), with 5-10% calcic labradorite ($\sim An_{70}$). Major oxide minerals (4-6%) are ilmenite and magnetite. Sulfides comprise 1 to 2 percent of the peridotite and are chiefly pyrrhotite, pentlandite, and chalcopyrite.

Ground magnetic, gravity, and very low frequency electro-magnetic surveys have refined the location and magnitude of anomalies previously known only from aeromagnetic studies. These surveys together with soil geochemical studies suggest that peridotite, and possibly other mafic rocks forming a differentiated igneous complex, may occur throughout a belt 20 km long (E-W) and 1-2 km wide (N-S).

Differentiated igneous complexes in many parts of the world are hosts for Cu, Ni, Cr, or precious metal deposits. The peridotite in the area of this study is anomalously rich in Cu and S compared to world-wide averages for peridotite. Positive electro-magnetic anomalies found near the peridotite outcrops may be caused by sulfide-rich zones in the igneous rocks and should be explored further for Cu-Ni mineralization.

Introduction

The Yellow Dog Plains in northern Marquette County, Michigan is a nearly featureless area underlain by Pleistocene sand and gravel and is nearly devoid of bedrock exposures. The bedrock beneath the plains is inferred to be mostly slate and other metasedimentary rocks of the Michigamme Formation, and has been shown as such on virtually all geologic compilations of the region. However, in sec. 11 and 12, T. 50 N., R. 29 W. are two outcrops of massive, partly serpentinized peridotite. The outcrops lie on and form the highest peaks of a west-trending linear aeromagnetic anomaly which is about 25 km long. (see fig. 1) That anomaly lies parallel to another anomaly of comparable magnitude about .5 to 1 km to the south. Both anomalies appear to cut the regional structural trends at low angles.

The two anomalies were first measured by Case and Gair (1965) and were inferred by them to be caused by magnetic sedimentary units in the Michigamme Formation. At that time the existence of the peridotite outcrops was not generally known. Because of the close association of the peridotite outcrops with the observed aeromagnetic anomalies and because the anomalies appear to cut across structural trends in the Michigamme Formation, we felt that both anomalies were associated with peridotite.

U.S. GOVERNMENT PRINTING OFFICE : 1972 O - 457-884

The relatively fresh, undeformed nature of the peridotite suggests that it is younger than the Penokean orogeny which deformed and metamorphosed other rocks in the area about 1.9 billion years ago. Because komatiitic magmas are not common in rocks younger than about 2.5 billion years and because the texture and chemical composition of the peridotite suggests that it is a crystal cumulate, we feel it is more likely that the peridotite is a differentiate from a less mafic magma rather than a product of a parental ultramafic magma.

The present study was undertaken to determine if a relatively large differentiated igneous complex is beneath the Yellow Dog Plains and, if so, to determine its configuration and potential for economic mineralization. An integrated program including ground magnetic, very low frequency electromagnetic (VLF-EM), gravity, paleomagnetic, rock chemistry and mineralogy and soil chemistry studies was carried out in 1976 as a cooperative project between the U.S. Geological Survey and the Geological Survey Division of the Michigan Department of Natural Resources. This report presents the results of that study and our inferences of the geology and mineral resource potential of the area of the Yellow Dog Peridotite and associated anomalies.

Acknowledgments.--R. Lilienthal, P. Geraci, and A. Grosz performed much of the geophysical field work, data reduction, and plotting. S. Quam assisted in interpreting and modeling the gravity data. Kenneth Books performed the magnetic susceptibility and remanence studies. M. P. Foose reviewed the manuscript.

General Geology

The region surrounding the Yellow Dog Peridotite contains Precambrian rocks of three ages. A gneiss-greenstone complex older than 2.5 billion years (Precambrian W) forms the basement for roughly 2 billion year old (Precambrain X) rocks of the Marquette Range Supergroup. The Marquette Range Supergroup is preserved in grabens in Precambrian W rocks formed during the Penokean Orogeny about 1.9 billion years ago (Cannon, 1973). Figure 1 shows the aerial distribution of Precambrian W and X rocks near Yellow Dog Plains. The plains, formed of Pleistocene sand and gravel, are underlain mostly by the Michigamme Formation, part of the Marquette Range Supergroup, in a structural trough known informally as the Baraga Basin. They are flanked by Precambrian W gneiss and greenstone on the north, east, and south. Because of the extensive Pleistocene cover in the basin little is known of the nature of the Michigamme Formation. Most exposures are along the southern flank of the basin where basal conglomerate, quartzite, and arkose as much as 20 m thick underly black slate and argillite. By projection of 10 km or more from areas of more abundant exposures to the west, most of the Michigamme in the study area is inferred to be fine-grained clastic rocks, largely black slate and argillite. These rocks were deformed and metamorphosed to the greenschist facies about 1.9 billion years ago, during the Penokean Orogeny.

The third age of Precambrian rocks is represented by west-trending diabase dikes of early Keweenawan age. The dikes were intruded and cooled during a period of reversed magnetic polarity about 1.1 billion years ago (Precambrian Y). Their negative remanent magnetization produces pronounced linear magnetic lows over the dikes and allows them to be identified and traced with certainty on aeromagnetic maps.

The Yellow Dog Peridotite is known from two exposures (see figure 1). Because it is undeformed and only moderately serpentinized, it was judged from field evidence to be younger than the Penokean orogeny that deformed and metamorphosed the surrounding Precambrian W and X rocks into which the peridotite was emplaced. Because the peridotite causes prominent positive aeromagnetic anomalies, it was initially believed that it was not related to lower Keweenawan diabase dikes that produce magnetic lows. Subsequent paleomagnetic studies by Kenneth Books of the U.S. Geological Survey, however, confirm that when the soft components of remanent magnetization are removed the peridotite does have a reversed remanent pole position very similar to that of other lower Keweenawan rocks in the region.

Petrology

Texture, mineralogy and bulk composition.--The peridotite is reddish brown on weathered surfaces and greenish black on fresh surfaces. The weathered rind is generally confined to a few millimeters of the surface. The rock is massive and coarse grained, without any visible layering, banding, or foliation. Poikilitic pyroxene is commonly a centimeter or more in length; olivine is generally 2 to 5 millimeters in diameter.

Microscopic examination indicates that the rock was originally a plagioclase lherzolite containing 40-50% olivine (now from 1/2 to 2/3 replaced by serpentine) and 20-30% pyroxene, with clinopyroxene generally slightly more abundant than orthopyroxene. Plagioclase comprises about 5-10% of the rock and chlorite is present in amounts ranging from 5-15%. Opaque minerals, discussed in more detail below, make up 4-8%. A variety of other minerals including both brown and green amphibole, red-brown biotite, sericite, talc, carbonate, clinozoisite, and rare colorless spinel(?) together comprise 5-10% of the rock.

U.S. GOVERNMENT PRINTING OFFICE: 1982 O - 377-094

Olivine occurs as euhedral phenocrysts, now partly altered to serpentine. Adjacent euhedral phenocrysts commonly are in contact with each other and appear to be accumulations of crystals that have settled from the magma rather than crystals that have grown in place, since there is no indication that the shape of the olivine grains is controlled by contact with adjacent grains. Olivine phenocrysts typically are surrounded by subhedral to anhedral pyroxene varying from about the same size as olivines to large grains poikilitically enclosing olivine phenocrysts. Some orthopyroxenes are euhedral, however, indicating crystal growth contemporaneous with olivine. Plagioclase generally occurs as subhedral and anhedral grains interstitial to pyroxene crystals. In a few places, it forms euhedral laths entirely within orthopyroxene, suggesting crystallization of at least some plagioclase prior to both pyroxene types. Green amphibole (actinolite) occurs as an alteration product of clinopyroxene and is clearly secondary. Brown hornblende forms rims on pyroxene grains and locally exhibits intercumulus textures suggesting a primary origin. Biotite occurs chiefly as subhedral laths which in places poikilitically enclose euhedral olivine. Most appears to have formed as an alteration of pyroxene, although the genesis of some euhedral intercumulus grains is not clear.

No cataclastic textures or other metamorphic fabrics are present on a microscopic scale. Minor deformation is displayed by shattered plagioclase grains and bent and kinked biotite flakes. The deformation may be due to volume expansion during the serpentinization of olivine (i.e., Hostetler and others, 1966; Coleman and Keith, 1971). Commonly the shattering of plagioclase is most intense where crystal terminations of serpentinized olivine grains impinge on plagioclase grains.

The origin of the peridotite is important in assessing the potential for contained mineral deposits. Economic Cu, Ni, and precious-metal ores are characteristically associated with layered mafic or ultramafic intrusions (i.e., Sudbury, Duluth), rather than with alpine-type intrusions. Utilizing criteria outlined by Thayer (1960), the Yellow Dog peridotite displays textural and mineralogical features strongly suggestive of a stratiform mafic-ultramafic genesis. If it is a product of a parental ultramafic magma (a komatiite) it might contain nickel sulfide deposits. If, on the other hand, it is a differentiate from a less mafic magma, disseminated copper-nickel sulfides, chromite, or precious metal ores could be present. The chemical composition of the peridotite (table 1) suggests that the rock is not a komatiite and that the present composition more likely is a result of differentiation from basaltic magma. Specifically, the high TiO_2/MgO ratio, and the low Al_2O_3 content for a corresponding FeO/FeO+MgO ratio shown by the peridotite are more characteristic of a tholeiite than of a komatiite, according to data summarized by Naldrett and Cabri (1976)and Arndt and others (1977). This together with the presence of cumulus olivine textures suggests that the bulk composition of the magma from which the peridotite crystallized was considerably less mafic than the present rock.

Composition of major primary silicate minerals.--Chemical analyses of olivines and pyroxenes were obtained with an ARL-EMX-SM electron microprobe operated at an accelerating potential of 15 KV and a beam current of 0.05 mA. Crystals used were ADP, LiF, and RAP, with 20-second counting intervals on 2-3 μm sized spots. Data reduction was performed by the method of Bence and Albee (1968). Two samples from the sec. 12 outcrop (fig. 2) were studied. Compositions in tables 2 and 3 represent means and standard deviations for 3 or more spots on several different grains for each slide.

Olivines (table 2) are chrysolites, Fo_{80-81}, and of similar composition from both samples. No significant differences in major or minor oxide content between samples is apparent. Orthopyroxenes (table 3) are enstatites, En_{77-79} Wo_{04} Fs_{17-19}, with only minor variations in composition between the two sample areas. The western sample (sample 7) contains orthopyroxenes slightly higher in FeO and TiO_2 and lower in MgO than sample 25. Clinopyroxenes are diopsidic augite, $En_{41,53}$ $Wo_{36,48}$ Fs_{11}, with identical FeO contents (6.5 wt. percent) for both samples. Significant compositional differences occur for TiO_2, Al_2O_3, MgO and CaO (table 3); Cr_2O_3 and Na_2O display minor variations between samples.

Compositions of individual silicate minerals are generally of limited use in determining parental magma type. The Yellow Dog peridotite contains olivines with 80-81 mole percent forsterite, a common composition for olivines found within many types of ultramafic rocks. Peridotitic komatiites typically contain more magnesian olivines, at Fo_{89-94} (Nesbitt, 1971; Pyke and others, 1973; Arndt and others, 1977). These compositions are not limited to komatiitic rocks, however, as cumulate parts of several layered mafic-ultramafic intrusions of tholeiitic origin (e.g., Stillwater) locally contain high-magnesian (>Fo_{90}) olivines. Other elements do not appear to be diagnostic indicators. Olivine compositions are thus of little use in distinguishing komatiitic from tholeiitic magma suites.

Chemical data for komatiitic pyroxenes are scarce, but one genetic discriminating parameter may be the alumina content of clinopyroxenes. Microprobe studies of ultramafic lavas from Ontario (Pyke and others, 1973; Arndt and others, 1977) and western Australia (Nesbitt, 1971) indicate unusually high contents of Al_2O_3 in clinopyroxene, generally from 5 to over 8 weight percent. Such alumina contents normally imply high formational pressure (Green, 1967), a condition clearly precluded by the subaerial environment of these lavas. High alumina contents of komatiitic clinopyroxenes are probably the result of disequilibrium crystallization during rapid quenching of ultramafic liquids under surface conditions. Nevertheless, most other ultramafic rocks formed at low pressures have low Al_2O_3 in clinopyroxene (O'Hara, 1967), providing an empirical method to distinguish tholeiitic from komatiitic magmas crystallized under volcanic and subvolcanic conditions. Clinopyroxenes from the Yellow Dog peridotite contain less than 3 wt. percent alumina, a feature compatible with bulk chemical data suggesting a tholeiitic rather than komatiitic affinity.

U.S. GOVERNMENT PRINTING OFFICE: 1977 O - 237-961

Differences in chemistry of clinopyroxenes for the two sample areas suggest somewhat different petrologic histories for the dikes. Modal proportions of olivine, orthopyroxene, and clinopyroxene are similar for both samples, such that variations in clinopyroxene composition reflect differences in crystal-melt equilibria during crystallization and/or slight differences in original bulk chemistry of magma between the two sites. The occurrence of primary calcic plagioclase ($\sim An_{70}$) coexisting with spinel (and hornblende ?) suggests low pressure conditions along the univariant breakdown curve between the orthopyroxene-plagioclase-lherzolite facies and the spinel-lherzolite facies (O'Hara, 1967; Frost, 1976). This assemblage is stable within a much higher P-T range than local greenschist facies rocks, thus reflecting original conditions of magma crystallization. Further work employing pyroxene geothermometers and geobarometers might closely define the petrogenesis of the peridotite.

Nickel contents of olivines and pyroxenes are opposite to predicted values based on experimentally determined distribution coefficients. In theory, olivines should contain much more nickel then coexisting pyroxenes. Recent detailed microprobe studies of similar Yellow Dog samples by W.J. Morris, Michigan State Univ. (written comm., 1977) suggests that the olivines contain about 0.4 weight percent Ni, roughly three times that of coexisting ortho and clinopyroxenes. We suspect an instrumental error in the anomalously low Ni values reported for our Yellow Dog olivines (table 2).

Opaque mineralogy.--Oxide and sulfide minerals typically make up 4 to 8 volume percent of the peridotite. Oxides are most abundant, and include ilmenite, magnetite, and minor to trace amounts of chromite and rutile. Ilmenite is the most common opaque, occurring as rounded to irregular skeletal grains up to 2 mm in size. Most are interstitial to olivine and pyroxene grains, but some are poikilitically enclosed by large pyroxene crystals. Ilmenite grains are generally fractured and show textures suggesting partial resorption. They characteristically occur isolated without associated oxides or sulfides. The majority of ilmenite grains are optically homogeneous, but some display fine, 1 to 3 μm-wide oriented [0001] lamellae of titanomagnetite and chromite (?). One presumably secondary inclusion of hematite was found along the margins of one ilmenite grain.

Magnetite occurs as both primary and secondary grains of variable size and shape. Primary magnetite is found as interstitial grains between silicates and as angular to rounded inclusions up to 0.5 mm in orthopyroxene. Secondary magnetite, formed by serpentinization of olivine and pyroxene, occurs as thin (5-10 μm) stringers between relict olivine crystals, and as isolated grains or clusters of grains surrounding or within altered pyroxenes. Some magnetite grains are complexly intergrown with sulfide minerals.

Chromite is a minor oxide phase found as polygonal to subrounded grains 0.1 mm in diameter, generally intergrown with relict olivine.

Trace amounts of rutile occur as irregular isolated grains 0.1 mm in length; one crystal displayed color zoning in transmitted light, with yellowish, orange, and dark red-brown bands.

Sulfide minerals typically comprise 1 to 2 percent of the peridotite. Major sulfides are pyrrhotite, pentlandite, and chalcopyrite, with minor pyrite and cubanite and trace amounts of mackinawite. Traces of secondary marcasite, bornite and covellite are present in a few sections. Sulfide minerals occur as composite grains up to 3 mm in diameter; the majority are less than 0.1 mm in size. Most are irregular in shape, fractured, and interstitial to silicates; some form 0.1 mm rounded inclusions or globules within pyroxene crystals. Sulfides show preferential association with magnetite, chiefly as chalcopyrite containing laths of magnetite. Less commonly, chalcopyrite occurs as myrmekitic intergrowths within certain magnetite grains. Cubanite and pentlandite generally occur with pyrrhotite or chalcopyrite. Complex intergrowths are common, mainly fine lamellae of chalcopyrite in cubanite and leaf-like blades of cubanite in pyrrhotite. Mackinawite occurs as small inclusions in cubanite.

U.S. GOVERNMENT PRINTING OFFICE : 1972 O - 457-684

Native nickel-iron alloy, probably awaruite, occurs as rare angular grains up to 15 μm in diameter, both in areas of secondary silicates such as serpentine and talc, and as isolated inclusions within olivine or pyroxene crystals. It is most likely the result of a reducing environment generated during serpentinization, producing native metals from decomposed silicates and altered sulfides (Eckstrand, 1975; Botto and Morrison, 1976).

Textures of certain oxide and sulfide phases suggest liquid immiscibility with the crystallizing peridotite. Sulfide globules within pyroxenes are likely the result of sulfur saturation and subsequent sulfide liquid separation. Rounded inclusions of magnetite in pyroxenes and myrmekitic magnetite-chalcopyrite intergrowths suggest contemporaneous immiscibility of oxides and sulfides from the silicate melt.

Trace element content.--Selected trace element contents from the Section 11 and 12 outcrops are given in table 4. Some elements show significant increases in concentration relative to world averages for peridotite and other ultramafic rocks (table 5). Most important are large anomalies for copper and sulfur, as well as zinc, and possibly silver[1]. Cobalt and nickel contents fall within typical ultramafic ranges; chromium is depleted by a factor of about two. Semiquantitative spectrographic analysis of 10 samples for 50 other elements failed, within detection limits, to identify any unusual metal concentrations.

[1] Varying limits of detection shown on table 5 preclude an accurate assessment of average Ag contents, but the presence of 0.2% Ag in four samples is clearly anomalous.

Copper contents of 37 samples of the Yellow Dog peridotite range from 90-350 ppm and average 150 ppm, compared to world-wide means of less than 50 ppm reported by various authors (table 5). The copper is not evenly distributed between the two outcrops, with the smaller sec. 11 outcrop considerably enriched relative to the sec. 12 outcrop, averaging 270 and 120 ppm, respectively. Copper values are clearly anomalous in relation to most other ultramafic rocks.

U. S. GOVERNMENT PRINTING OFFICE: 1972 O - 457-044

Sulfur is also distinctly higher within Yellow Dog Plains samples than average ultramafic rock (table 5). The most recent compilation of Wedepohl (1975) suggests 400 ppm (0.04%) as a mean sulfur value for ultramafic rocks. Four Yellow Dog peridotite samples yielded a range of from 0.070 to 0.174 wt. percent S, with an average of 0.134. Sulfur and copper contents may be used as effective discriminators of ore potential, according to the method of Cameron and others (1971). The sulfur contents of over 1000 ultramafic rocks of the Canadian Shield were grouped by them into barren, minor ore, and ore categories, based on Cu-Ni production figures. Barren ultramafics (N=616 samples) display sulfur contents ranging from 0.011 to 0.327 wt. %, with a mean of 0.059 and standard deviation of 0.107. Minor ore samples (N=91) vary from 0.029 to 0.879, with a mean and standard deviation of 0.177 and 0.559, respectively. Ultramafic rocks associated with 16 major Cu-Ni ore deposits (N=372) contain from 0.112 to 1.92%S, with a mean of 0.582 and standard deviation of 1.37. Although there is much scatter in the data, sulfur contents of Yellow Dog peridotite are most similar to the minor ore category, as defined by Cameron and others (1971). Nickel and cobalt contents of major ore suites are not significantly enriched relative to typical ultramafic rocks (Cameron and others, 1971, p. 308), a pattern followed by Yellow Dog samples (table 5). Notably, copper was found to be the second most important discriminator of ore potential, after sulfur. Anomalously high copper and sulfur contents determined for Yellow Dog Plains samples suggest the possibility of economic Cu-Ni mineralization at depth.

Paleomagnetic Studies

Seven hand specimens were collected from the two outcrops of the peridotite. Two cores from each sample were analyzed by Kenneth Books of the U.S. Geological Survey in the Reston magnetic laboratory. Measurements were made for susceptibility, direction and intensity of remanence. Susceptibility was converted to intensity of induced magnetism. Remanence data for natural remanent magnetization and for succeeding steps of alternating current cleaning up to 500 oersteds were computer analyzed and a Fisher statistical analysis run for each step. The optimum cleaning step (least scatter of direction) appeared to be at 200 oersteds but even at that step the samples showed considerably more scatter than other lower Keweenawan rocks previously analyzed from the region. The virtual geomagnetic pole data are: latitude -58.68; longitude 142.62 east; delta m=38.58; and delta p=34.29. The "optimum" cleaned direction of magnetization for the peridotite is not significantly different statistically from some other lower Keweenawan directions of magnetization and is very similar to directions obtained for diabase dikes nearby (DuBois, 1962). The peridotite can confidently be assigned a lower Keweenawan age.

The relatively large scatter and differing polarizations of the natural remanent magnetization obtained from different samples indicate secondary components of magnetization. These components may be at least partially responsible for the net north-seeking down magnetization in the peridotite and could produce the positive magnetic anomaly over the peridotite. Although probably small, another contributor to a positive anomaly over the peridotite might be the moderate intensity of the induced magnetization (2.50×10^{-3} emu/cm^2). This induced magnetization may be compared to the average intensity of remanent magnetization for the seven samples of 69.20×10^{-3} emu/cm^2.

It is possible that secondary magnetite produced during serpentinization of part of the olivine has a normal remanent direction and is at least partly responsible for the scatter of pole positions and the positive magnetic anomaly.

U.S. GOVERNMENT PRINTING OFFICE: 1982 O-362-993

Field Geophysical Studies

Field geophysical studies consisted of detailed surveys near the peridotite outcrops in sec. 11 and 12, T. 50 N., R. 29 W. and more widely spaced survey lines along an east-west belt about 20 km long and at a greater distance from the outcrops. Gravity, ground magnetic, and very low frequency electromagnetic (VLF-EM) techniques were all used in the detailed survey area. Ground magnetic and VLF-EM profiles were measured along selected lines in the less detailed area (see figure 5). The combined use of all three geophysical techniques greatly restricts the spectrum of possible geologic bodies responsible for the measured anomalies and allows a closer approach to a unique solution than would be possible with any single technique. Complications of interpretation arise, however, due to several factors. Most important are the complexities of the magnetic field caused by the interaction of the induced field and the irregularly oriented natural remanent field, the possible variations in density of the peridotite due to variable degrees of serpentinization, imprecise knowledge of the densities of all rock types in the area, and the imprecise understanding of the requirements for a rock body to produce a measurable VLF-EM response. In spite of these difficulties much useful information has been obtained on the geologic nature of the area and two alternate models seem consistent with the observed geological and geophysical data.

Field procedures and data reduction

Gravity.--Figure 3 shows the gravity coverage in the detailed study area and the location of two regional profiles. In the detailed study area nine gravity profiles spaced 400 m apart were measured in an north-south direction, roughly perpendicular to the trend of the aeromagnetic anomaly. Station spacing on the profiles was 152 meters. The two regional profiles cross the southernmost aeromagnetic anomaly as well as the north anomaly.

Gravity values were measured with a LaCoste and Romberg model G land gravimeter. Drift checks, taken at bench mark 1422 every three hours or less, had less than 0.1 miligal drift per hour. The gravity readings were tied to the Marquette gravity base by the base loop method.

Most elevations were determined by leveling between U.S. Geological Survey benchmarks. North of the base line (see figure 3) surveys closed within 5 cm; south of the baseline, where swamps made surveying difficult, elevation surveys closed within 18 cm or better. A few elevations shown on figure 3 were determined by altimeter with an estimated accuracy based on repeated readings of 1.6 m or less. All distances were measured with a steel tape and have an estimated accuracy of 3 m or less.

The gravity data were reduced using the 1967 international gravity formula, a 427 m above sea level datum, and a bouguer density of 1.7 g/cm^3. The 1.7 g/cm^3 value is the density of the sand and silt that covers the bedrock and was determined from a density profile measured over a small topographic feature in the sand plains.

Ground magnetics.--Figure 4 shows the ground magnetic coverage in the detailed study area as well as several profiles that were extended southward into sec. 18 and 14. North of the base line seventeen profiles were measured; south of the base line ten profiles were measured. Station spacing along the profiles was 30.3 meters. North of the base line station spacing was measured with a steel tape and south of the base line distances were determined by pace.

Figure 5 shows the regional ground magnetic coverage. Outside of the detailed study area twenty profiles were measured with spacing between profiles from 800 to 1200 m. Five profiles from figure 4 are included in figure 5 to maintain continuity of coverage. Station spacing for these profiles was 30.3 m determined by pace.

All readings were taken with a Geometrix model G816 proton precession magnetometer in the backpack mode. Base checks for magnetic drift were made at bench mark 1422 every three hours or less. Data were discarded if the magnetic drift exceeded 20 gammas per hour.

Inasmuch as all data were tied to a common base, this base served as a reference for the magnitude of the total magnetic field in this area. It was assigned a value of 59,780 gammas based on the average of 25 readings which had a total range of 60 gammas (59,766 to 59,826 gammas).

VLF-EM.--VLF-EM coverage in the detailed study area consisted of 16 lines shown on figure 6. All readings were taken with a Geonics EM-16 unit facing north. The station spacing along the profiles was 30 m determined by pace. Transmitter locations used in the survey were NLK, Seattle, Washington (18.6 kHz) and NAA Cutler, Maine (17.8 kHz).

Regional VLF-EM coverage consisted of two lines located on figure 5. Line 1 is the southern extension of the westernmost line in the detailed study area. It was extended to cross the southernmost aeromagnetic anomaly. Line 3 located 9 km west of the detailed study area crossed both the northern and southern aeromagnetic anomalies. Station spacing on both lines was 30 m determined by pace.

To make the VLF-EM data easier to interpret and to smooth noisy data, all of the profiles, including both the in-phase and quadrature components, were filtered by a method outlined by Fraser (1969). The filter is a difference operator and low-pass filter that smooths the data and transforms zero crossovers into peaks and troughs, depending on the direction of the crossover. These filtered data are then contoured into positive and negative anomalies as shown on figure 6.

Interpretation of geophysical data

Area of detailed survey.

Within the area studied in detail several anomalies were located by VLF-EM surveys. They are shown in figures 6 and 7 and table 6 lists the geophysical and geological character of each. At and near the peridotite outcrops negative filtered in-phase anomalies were found (B_n and C_n on figures 6, 7) but several other linear anomalies, both positive and negative, were also found.

With the VLF-EM technique either positive or negative anomalies are obtained when the raw data is filtered. Positive in-phase anomalies, which ideally have a positive peak flanked by nearly symmetrical negative shoulders (see VLF-EM anomaly B_p on figure 6), generally indicate the presence of anomalous conductivity. Negative in-phase anomalies ideally have a pronounced trough with nearly symmetrical positive shoulders (see anomaly B_n on figure 6). Negative VLF-EM anomalies may be caused when: A) a resistive body is located in a field or more conductive material, such as a resistive dike outcropping in a swamp or area of conductive clay (Ronka, Patterson, written communication), or B) when a dike with a high magnetic permeability and a low degree of conductivity causes a response in the VLF-EM receiver coils due to the natural magnetic field overiding the electromangetically induced field (Grant and West, 1965). The second situation appears to be the case in this study because the negative in-phase anomalies occur over the highly magnetic peridotite outcrops in an area of thick dry sand rather than conductive swamp. The peridotite outcrops and all other areas of negative VLF-EM anomalies have pronounced positive magnetic anomalies whereas the positive VLF-EM anomalies have little or no magnetic expression.

Thus, two types of anomaly-causing bodies seem to be present in the area. Peridotite bodies produce strong positive magnetic anomalies and negative in-phase VLF-EM anomalies (A_n, B_n, C_n). Other bodies of unknown nature produce positive in-phase VLF-EM anomalies but have little or no magnetic expression (A_p, B_p, D_p). It is believed that these VLF-EM anomalies are caused by bodies that are genetically related to the peridotite, because they have a close spatial relationship to the peridotite and trend parallel to the negative in-phase anomalies caused by the peridotite.

Gravity measurements, discussed in more detail below, indicate that all anomaly-producing bodies are denser than the granitic and metasedimentary rocks of the area.

An additional positive EM anomaly (C_p) trends at a high angle to the other anomalies and is believed to be caused by a fault zone. The positive anomaly may be caused by electrolytic solutions or metallic mineralization in the shear zone of the fault. The rather low intensity of anomaly C_p may be a result of the strike of the causative body being at a high angle to the survey direction and not perpendicular to the nearly north-south transmitted electromagnetic field direction so that a less than maximum coupling of the conductor with the transmitted field was achieved.

The fault zone is also expressed by discontinuities in the magnetic and gravity anomalies. Most data suggest that the zone is about 500 meters wide and occupies most of the area between the two peridotite outcrops. Another northwest-trending fault is inferred from the ground magnetic data (figure 7) near the west edge of sec. 11. The northwest extension of VLF-EM anomaly B_p is probably caused by this fault.

The positive gravity anomaly in the detailed survey area (see figure 3) indicates a considerable excess of mass over that which could be caused by metasedimentary rocks of the Michigamme Formation. Two alternative density models have been constructed that are consistent with both the regional geological relationships and the detailed geophysical data.

Two residual gravity anomalies were graphically separated from the Bouguer anomaly by the cross profile method. Figure 8 illustrates the three components into which the gravity anomaly was divided. Residual 1 (figure 9) is a broad anomaly probably caused by a horizontal discontinuity in density at depth. Residual 2 (figure 10) is a narrower anomaly caused by the peridotite and possibly other dense rock bodies at least partially near the surface. Two-dimentional density models were contructed (AA' and BB', figure 11) to produce a theoretical gravity profile by the Talwani two-dimensional method (Talwani and others, 1959) that matches the observed gravity anomaly. The two alternative models are discussed separately.

Basement fault model.--In the basement fault model (see figure 11A) the broad low frequency gravity anomaly is a result of relative uplift of Precambrian W basement rock (density 2.8 g/cm^3) along a west-trending fault so that on the southern downthrown side the Michigamme Formation (density 2.7 g/cm^3) is thicker than on the north. If these densities are correct, a vertical displacement of about 750 meters is required to produce the gravity anomaly. The higher frequency anomaly is produced by peridotite (density 2.9 g/cm^3) and other rocks of similar density in vertical dikes. The position of the dikes is consistent with ground magnetic and EM anomalies. The dikes are localized near the west-trending fault and trend parallel to it. The geology of this model is similar to that in other better known areas nearby where basement faults are well mapped and their subsurface configuration has been determined by gravity studies (Klasner and Cannon, 1974; Cannon and Klasner, 1977).

Mafic sheet model.--The gravity field can also be reproduced by a model in which a thick sheet of mafic rocks (density 2.9 g/cm^3) lies at depth (see figure 11B). The low frequency anomaly is caused by the mafic sheet rather than a basement fault. The narrower anomaly is caused by dikes with the same configuration as those in the basement fault model. No mafic sheets are known in the region but this model does suggest a possible source body from which the peridotite may have formed by fractional crystallization and differentiation. The magnetic data gives no evidence of the presence of a mafic sheet but because of the complexities in remanent magnetism, firm conclusions cannot be made.

Interpretation of individual VLF-EM anomalies.

The map of VLF-EM anomalies (figures 6, 7) shows that there are three positive anomalies, A_p, B_p, D_p, in addition to the fault-induced positive anomaly C_p. Anomaly A_p has the highest amplitude of the positive anomalies. It is probably offset by a small northwest trending fault. Gravity model AA' shows that it can be caused by a 15 m thick dike. Because it does not have an associated ground magnetic anomaly, the causitive material may be something other than peridotite, and the anomalous conductivity indicated by the positive VLF-EM anomaly, suggests that it may contain sulfide mineralization. Depth estimates are 37 m to the top of the conductive body from VLF-EM data and 91 meters to the top of a dike from gravity data (see figure 11).

VLF-EM anomaly B_p is probably a compound anomaly. The high intensity part of the anomaly (20 arbitrary filtered units) may be due, in part, to clay and electrolyte solutions in the underlying swamp. However, profile 1000W (figure 6) has a negative in-phase/quadrature relationship which may indicate a subsurface conductor other than the swamp. This is supported by gravity model BB' which shows a 61 m thick dike at B_p near line 600W. There is only a slight magnetic anomaly over the dike indicating small amounts of magnetite but the positive EM anomaly indicates the possibility of sulfide mineralization. VLF-EM data on line 1000W indicates the conductive body is 45 meters below the surface. Near line 600W the gravity data indicate the top of the dike is about 30 meters below the surface.

VLF-EM anomaly D_p has a maximum intensity of slightly more than ten arbitrary units. It falls within an area of a slight positive gravity anomaly but has no magnetic expression. VLF-EM data indicate the top of the causitive body is about 30 meters below the surface. The nature of the causitive body is not known.

It is possible that the three positive VLF-EM anomalies, A_p, B_p, and D_p, could be caused by conductive zones such as graphitic layers within the metasedimentary rocks of the Michigamme Formation. However, the gravity data indicate excess mass in the anomalous zones, therefore supporting the interpretation of sulfide mineralization rather than graphite as the cause of the anomalous conductivity.

There are three negative anomalies in the filtered VLF-EM data, A_n, B_n, and C_n on figure 6. Anomaly A_n is continuous in an east-west direction for about 2800 meters, the total extent of the detailed study area. Locally it has an intensity of 20 units which may be due to the causitive body being very near the surface. The anomaly is very weak in the area of the northwest-trending fault zone (lines 00 and 200E). A_n is coincident with a magnetic anomaly (compare with figure 4 and see gravity models AA' and BB'). Gravity data indicate that the causitive body is a vertical dike about 30-45 meters thick. As with all of the negative VLF-EM anomalies, the combined VLF-EM and magnetic data indicate that the causative bodies have high magnetic permeability, probably caused by magnetite.

Negative VLF-EM anomaly B_n has the highest absolute intensity of any of the EM anomalies. It overlies a peridotite outcrop but is much larger in area than the outcrop. It is coincident with an intense (1,700 gammas above beckground) ground magnetic anomaly. Gravity model AA' shows that the causative feature may be a vertical dike about 90 meters thick. All geophysical data indicate that the dike ends abruptly near the west edge of the outcrop. It is probably truncated by a northwest-trending fault.

VLF-EM anomaly Cn is also associated with a peridotite outcrop. The anomaly trends east-west and is much narrower and smaller in amplitude than B_n. Gravity model BB' indicates that it may be caused by a 30 m thick vertical dike. This dike is also abruptly terminated at the northwest-trending fault zone.

U.S. GOVERNMENT PRINTING OFFICE : 1972 O - 472-064
667-1

Regional Survey

Regional geophysical coverage outside of the area of the detailed survey was designed to accomplish two things: 1) to test the continuity of the inferred dikes in an east-west direction, and 2) to examine the VLF-EM response in the area of the aeromagnetic anomalies at three locations (profiles 1, 2, 3, figure 5).

The continuity of the magnetic anomalies away from the area of the peridotite outcrops is illustrated in figure 5. The anomalies can be traced for about 20 km and are approximately coincident with the aeromagnetic anomalies of Case and Gair (1965), thus suggesting that a swarm of dikes, at least some of which are peridotite, underly the area. The southernmost inferred dike on figure 5, which corresponds to the southern aeromagnetic anomaly, is at least 8 km long. Other dikes do not appear to be as long although the discontinuous nature of some of the anomalies may be due to post-Keweenawan faulting, to variations in the magnetic mineral content, or changes in the remanent magnetism along the strike of the dikes.

Figure 12 shows two of the regional profiles measured to obtain more information on the nature of the aeromagnetic anomalies. Profile 1 extends south from the base line near the western edge of the detailed study area for 2400 meters and crosses the southern aeromagnetic anomaly. There is no VLF-EM response over the aeromagnetic anomaly but ground magnetic measurements confirm the presence of the aeromagnetic anomaly. We interpret these data to indicate that a magnetic dike is present but is too deep to be detected by VLF-EM measurements.

The absence of a gravity anomaly in the area indicates either that the dike is very thin or has a density close to that of the surrounding rocks.

Regional profile 2 is not shown on figure 12 but is incorporated into the gravity and magnetic maps (figures 3 and 4). The profile is similar to profile 1 and our interpretation of the anomalies is the same as for profile 1.

Regional profile 3 (figure 12) starts at a road intersection in the NE 1/4, SW 1/4, sec. 11, T. 50 N., R. 30 W. and extends for 2424 m to the north, across the two aeromagnetic anomalies. Ground magnetic measurements on this profile confirmed the presence of the two aeromagnetic anomalies and also showed anomalous readings near the south end of the profile. In all there are five VLF-EM anomalies (A through E on figure 12) that warrant discussion.

Anomaly A.--This anomaly has a corresponding ground magnetic anomaly and a negative in-phase VLF-EM anomaly. The in-phase/quadrature relationship suggests that the filtered EM anomaly may not be real. Further electromagnetic studies are needed to test for the presence of an anomalous body at this point.

Anomaly B.--The filtered VLF-EM data indicate the presence of an underlying relatively flat, wide (545 m) conductive body. Ground magnetics show a slight positive anomaly near the south edge of the body, but otherwise the magnetic profile is featureless in this area. The VLF-EM data indicate the causitive body is about 30 meters below the surface. The anomaly may be caused by graphitic slate.

Anomalies C, D, and E.--These three VLF-EM anomalies are negative and lie near the edges of the ground magnetic and aeromagnetic anomalies. The cause of the anomalies is not known but could be either resistive dikes or a rock with high magnetic permeability.

U. S. GOVERNMENT PRINTING OFFICE : 1982 O - 377-994

Geochemical Survey

Because the peridotite is much richer in certain elements such as Cu, Ni, Co, Zn, Cr, and Mg, than the surrounding rocks, geochemical analysis of soils in areas of the positive aeromagnetic anomalies might give additional confirmation of the presence of buried peridotite. Near the peridotite outcrops and in most of Yellow Dog Plains the Pleistocene drift cover is relatively thick and is mostly porous stratified sand and gravel. Chances that a geochemical anomaly from buried bedrock would be present in soil developed on the drift are slight and such areas were not tested. The westernmost extension of the magnetically anomalous area has thinner drift cover and the drift is mostly till. In that area it was believed chances were good to detect anomalous bedrock compositions by soil analyses.

Samples were collected along north-south traverses shown in figure 13 that crossed both the northern and southern aeromagnetic anomalies. Samples were taken roughly 40 cm below the surface, generally below the organic-rich upper soil horizons. Most of the material sampled was reddish brown sandy soil. In the laboratory the samples were sieved and the minus 80 mesh fraction was analyzed for 65 elements by a semi-quantitative spectrometric technique at the U.S. Geological Survey analytical laboratories in Reston, Virginia.

The results show that weak geochemical anomalies occur at or near the magnetic anomalies on two of the three profiles (profiles A and B, Fig. 13). The third profile (C) had no anomalies but is mostly on thick sand deposits of the Yellow Dog Plains through which effective geochemical communication between soil and bedrock is unlikely. Figures 14 and 15 show the content of elements along profiles A and B. On profile A a broad anomalous area with higher than average values for Co, Cu, Ni, and Zn coincides with the northernmost aeromagnetic anomaly. A narrower, weaker anomaly in these elements is suggested near the southernmost aeromagnetic anomaly. Ag and Cr also appear to be slightly anomalous in the areas of the magnetic anomalies. Likewise on profile B there are two separate anomalous areas. A weak Co, Cu, Ni anomaly is near the northernmost aeromagnetic anomaly. A more pronounced anomaly in Ag, Co, Cu, Ni, and Zn is about 0.4 km south of the southernmost magnetic anomaly. There is a suggestion of higher than average Cr with both anomalies but the relationship is weak. The southernmost anomaly on B also has higher than average Mg content but the three remaining anomalies do not have high Mg values. This may indicate that the anomalies are caused mostly by elements such as Cu, Co, Ni, and Zn being released from sulfide minerals during weathering whereas Mg and Cr, although abundant in the peridotite or mafic rocks are held in less readily weathered silicate or oxide minerals.

Earlier work by the U.S. Geological Survey in the region immediately west of the area of this study disclosed weak soil anomalies that are clearly related to weakly anomalous zones in the Michigamme Formation. There the anomalies in both bedrock and soil are expressed by all or some of the elements that are anomalous on profiles A and B plus Pb and Mo. The soil anomalies A and B do not have anomalous Pb and Mo values and Cr appears more consistently high there than in anomalies related to the Michigamme Formation. The suite of anomalous elements in profiles A and B mirrors the element distribution of peridotite more closely than the element distribution in the Michigamme Formation.

Highly differentiated mafic rocks can be hosts for a variety of ore deposits including Cu, Ni, Cr, and precious metals. The peridotite in the two outcrops contains an average of 150 ppm Cu and some samples contain as much as 355 ppm. Sulfur contents range from .07 to .174%. It is considerably richer in both copper and sulfur than average peridotite and in that respect resembles ore-bearing peridotites in other parts of the Canadian Shield. Positive EM anomalies, such as A_p and B_p, in areas of positive gravity anomalies may be caused by zones of sulfide concentrations in peridotite or mafic rocks and need further study to determine the nature of the conductive body. Should the anomalies be shown to be caused by sulfide mineralization, the 20 km long magnetically anomalous zone would be a well defined exploration target for extensions of that mineralization.

The Yellow Dog peridotite is the only lower Keweenawan peridotite known in northern Michigan. Its tectonic significance is not yet known. Paleomagnetic data indicate that it is approximately the same age as the Duluth Complex in Minnesota. Prior to middle Keweenawan rifting it was much closer to the Duluth Complex than it now is. Perhaps there is a genetic relationship between the Yellow Dog and Duluth rocks. If the two are comagmatic the Yellow Dog Peridotite may be a favorable host rock for copper-nickel mineralization similar to that in parts of the Duluth complex.

U.S. GOVERNMENT PRINTING OFFICE: 1972 O - 472-964

Summary and Conclusions

Peridotite of early Keweenawan age is exposed at two outcrops in Sec. 11 and 12, T. 50 N., R. 29 W. in an area generally mantled by Pleistocene outwash and till. Geophysical studies indicate that the peridotite is an east-west elongate body at least 1.5 km long. Gravity, ground magnetic, and VLF-EM surveys have disclosed several other anomalies nearby with the same trend as the peridotite. Some of these anomalies extend at least 15 km west and 5 km east of the peridotite outcrops and are coincident with a 20 km long aeromagnetically anomalous zone consisting of two parallel positive anomalies about 1 km apart.

Eight to 12 km west of the outcrops geochemical soil anomalies of several elements abundant in the peridotite are coincident with the aeromagnetic positive anomalies and may indicate that peridotite extends that far west. Therefore, with decreasing degrees of certainty peridotite and related rocks can be inferred in a belt from as little as 1.5 to as much as 20 km long.

The peridotite from the outcrops is believed from both chemical composition and texture to be a differentiate from a less mafic magma rather than a komatiite-like ultramafic rock. Thus, it seems likely that a larger body of mafic rock from which the peridotite has formed by fractional crystallization and differentiation lies buried somewhere in the region. A broad, low frequency and low amplitude gravity anomaly near the peridotite outcrops may be caused by such a body at depth.

References

Arndt, N. T., Naldrett, A. J., and Pyke, D. R., 1977, Komatiitic and iron-rich tholeiite lavas of Munro Township, northeast Ontario: Jour. Petrology, v. 18, p. 319-369.

Bence, A. E., and Albee, A. L., 1968, Empirical correction factors for the electron microanalysis of silicates and oxides: Jour. Geology, v. 76, p. 382-403.

Botto, R. I., and Morrison, G. H., 1976, Josephinite: A unique nickel-iron: Am. Jour. Sci., v. 276, p. 241-274.

Cameron, E. M., Siddeley, G., and Durham, C. C., 1971, Distribution of ore elements in rocks for evaluating ore potential: nickel, copper, cobalt, and sulphur in ultramafic rocks of the Canadian Shield: Can. Inst. Min. Spec. Volume 11, p. 298-313.

Cannon, W. F., 1973, The Penokean orogeny in northern Michigan: Geol. Assoc. Canada, Special Paper 12, p. 251-271.

_____, and Klasner, J. S., 1977, Geologic map and geophysical interpretation of the Witch Lake Quadrangle, Michigan: U.S. Geol. Survey Misc. Inv., map I-987.

Case, J. E., and Gair, J. E., 1965, Aeromagnetic map of parts of Marquette, Dickinson, Baraga, Alger and Schoolcraft Counties, Michigan and its geologic interpretation: U.S. Geol. Survey map GP-467.

U.S. GOVERNMENT PRINTING OFFICE: 1978 O - 677-664

Coleman, R. G., and Keith, T. E., 1971, A chemical study of serpentinization--Burro Mountain, California: Jour. Petrology, v. 12, p. 311-328.

Dubois, P. M., 1962, Paleomagnetism and correlation of Keweenawan rocks: Canada Geol. Survey Bull. 71, 75 p.

Eckstrand, O. R., 1975, The Dumont serpentinite: A model for the control of nickeliferous opaque mineral assemblages by alteration reactions in ultramafic rocks: Econ. Geology, v. 70, p. 183-201.

Fisher, D. E., Joensuu, O., and Boström, K., 1969, Elemental abundances in ultramafic rock and their relation to the upper mantle: Jour. Geophys. Res., v. 74, p. 3865-3873.

Fraser, D. C., 1969, Contouring VLF-EM data: Geophysics, v. 34, p. 958-967.

Frost, B. R., 1976, Limits to the assemblage forsterite-anorthite as inferred from peridotite hornfelses, Icicle Creek, Washington: Am. Mineralogist, v. 61, p. 732-750.

Goles, G. G., 1967, Trace elements in ultramafic rocks in Wyllie, P. J., ed., Ultramafic and Related Rocks: John Wiley and Sons, New York, p. 352-362.

Grant, F. S., and West, F. G., 1965, Interpretation theory in applied geophysics: McGraw-Hill Book Co., N. Y.

Green, D.H., 1967, High-temperature peridotite intrusions in Wyllie, P. J., ed., Ultramafic and Related Rocks, John Wiley and Sons, New York, p. 212-222.

U. S. GOVERNMENT PRINTING OFFICE : 1972 O - 747-934

Hostetler, P. B., Coleman, R. G., Mumpton, F. A., and Evans, B. W., 1966, Brucite in Alpine serpentinites: Am. Mineralogists, v. 51, p. 75-98.

Klasner, J. S., and Cannon, W.F., 1974, Geologic interpretation of gravity profiles in the western Marquette district, Northern Michigan: Geol. Soc. America Bull., v. 85, p. 213-218.

Naldrett, A. J., and Cabri, L. J., 1976, Ultramafic and related mafic rocks: Their classification and genesis with special reference to the concentration of nickel sulfide and platinum-group elements: Econ. Geol., v. 71, p. 1131-1158.

Nesbitt, R. W., 1971, Skeletal crystal forms in the ultramafic rocks or the Yilgarn block, western Australia: Evidence for an Archaen ultramafic liquid: Geol. Soc. Australia Spec. Pub. 3, p. 331-347.

O'Hara, M. J., 1967, Mineral facies in ultrabasic rocks in Wyllie, P. J., ed., Ultramafic and Related Rocks: John Wiley and Sons, N. Y., p. 7-18.

Pyke, D. R., Naldrett, A. J., and Eckstrand, O. R., 1973, Archean ultramafic flows in Munro Township, Ontario: Geol. Soc. American Bull., v. 84, p. 955-978.

Talwani, M., Worzel, J. L., and Landisman, M. G., 1959, Rapid gravity computations for two-dimensional bodies with application to the Mendocino submarine fracture zone: Jour. Geophys. Research, v. 64, p. 49-59.

U. S. GOVERNMENT PRINTING OFFICE : 1972 O - 457-804

Thayer, T. P., 1960, Some critical differences between alpine-type and stratiform peridotite-gabbro complexes: 21st. Intern. Geol. Congr., Copenhagen, Repts., Pt. 13, p. 247-259.

Turekian, K. K., and Wedepohl, K. H., 1961, Distribution of the elements in some major units of the Earth's crust: Geol. Soc. Am. Bull., v. 72, p. 175-192.

Vinogradov, A. P., 1962, Average contents of chemical elements in the principal types of igneous rocks of the Earth's crust: Geochemistry no. 7, p. 641-664.

Wedopohl, K. H., 1975, The contributions of chemical data to assumptions about the origin of magmas from the mantle: Fortschr. Miner., v. 52, p. 141-172.

Table 1.--Chemical analyses of the Yellow Dog Peridotite

	#6	#35
SiO_2	45.0	40.2
TiO_2	.83	.92
Al_2O_3	4.4	6.0
Fe_2O_3	14.3	6.4
FeO	(total Fe)	7.7
MnO	.18	.18
MgO	24.9	24.9
CaO	4.4	3.1
Na_2O	.36	.40
K_2O	.11	.20
P_2O_5	.10	.046
F	n.a.	.03
LOI[1/]	5.56	7.8
Moisture (105°C)	n.a.	.01
CO_2	n.a.	.1
Total	100.15	97.99

n.a. - not analyzed

1/ LOI - loss on ignition at 1,000°C

#6 - is from sec. 12 outcrop and was analyzed at Rocky Mtn. Geochem. Corp.

#35 - is from sec. 11 outcrop and analyzed at Skyline Labs Inc.

Table 2.--Electron microprobe analyses of olivines from the Yellow Dog Peridotite

	Sample Number	
Oxide Wt %	YDP-7	YDP-25
SiO_2	38.88 ± .76	39.90 ± .41
TiO_2	0.04 ± .04	0.01 ± .00
Al_2O_3	0.05 ± .04	0.04 ± .02
FeO*	18.44 ± .93	17.81 ± .83
Cr_2O_3	0.05 ± .04	0.03 ± .03
MnO	0.21 ± .08	0.20 ± .04
NiO	0.01 ± .02	0.00 ± .00
MgO	40.74 ± .79	42.21 ± .58
CaO	0.22 ± .09	0.26 ± .05
Na_2O	0.01 ± .01	0.02 ± .02
Total	98.65	100.48

* Total iron as FeO

	Numbers of ions on basis of 4 Oxygens	
Si	1.010	1.010
Al	0.001	0.000
Ti	0.000	0.000
ΣFe	0.400	0.380
Cr	0.000	0.000
Mg	1.570	1.590
Ni	0.000	0.000
Mn	0.004	0.004
Ca	0.005	0.006
Na	0.000	0.000
Total	2.990	2.990

Table 3.--Electron microprobe analyses of pyroxenes from the Yellow Dog Peridotite.

	Orthopyroxenes		Clinopyroxenes	
Oxide Wt %	YDP-7	YDP-25	YDP-7	YDP-25
SiO_2	54.26 ± .59	55.24 ± .63	51.90 ± .55	51.71 ± .34
TiO_2	0.57 ± .05	0.40 ± .10	0.45 ± .12	1.45 ± .10
Al_2O_3	1.55 ± .25	1.84 ± .44	1.85 ± .37	2.71 ± .16
FeO*	12.17 ± .22	11.33 ± .48	6.53 ± .58	6.52 ± .17
Cr_2O_3	0.32 ± .07	0.37 ± .08	0.92 ± .07	0.56 ± .05
MnO	0.25 ± .05	0.20 ± .04	0.13 ± .04	0.16 ± .03
NiO	0.11 ± .14	0.02 ± .03	0.09 ± .09	0.04 ± .07
MgO	27.84 ± .40	29.02 ± .31	18.49 ± .21	16.29 ± .13
CaO	1.99 ± .14	1.90 ± .17	17.57 ± .92	19.25 ± .39
Na_2O	0.05 ± .04	0.04 ± .02	0.29 ± .02	0.43 ± .04
Total	99.11	100.36	98.22	99.12

*Total iron as FeO

Table 3 (Cont'd).--Electron microprobe analyses of pyroxenes from the Yellow Dog Peridotite.

	Numbers of ions on basis of 6 oxygens			
Oxide Wt %	YDP-7	YDP-25	YDP-7	YDP-25
Si	1.953	1.952	1.934	1.914
Al	0.065	0.076	0.080	0.117
Ti	0.015	0.010	0.012	0.040
ΣFe	0.366	0.334	0.203	0.201
Cr	0.008	0.010	0.027	0.016
Mg	1.493	1.528	1.025	0.898
Ni	0.003	0.000	0.002	0.001
Mn	0.007	0.005	0.004	0.004
Ca	0.076	0.071	0.700	0.763
Na	0.003	0.002	0.020	0.030
Total	3.989	3.988	4.007	3.984

U. S. GOVERNMENT PRINTING OFFICE : 1972 O - 457-084
667-100

Table 4.--Trace element content of the Yellow Dog Peridotite (ppm)

Sample	Ag	Cu	Co	Cr	Ni	Zn
1	n.a.	160	n.a.	n.a.	1400	n.a.
2	n.a.	145	n.a.	n.a.	1400	n.a.
3	n.a.	335	n.a.	n.a.	1700	n.a.
4	n.a.	115	n.a.	n.a.	1200	n.a.
5	n.a.	340	n.a.	n.a.	1700	n.a.
6	n.a.	125	n.a.	n.a.	1300	n.a.
7	<.2	90	50	3000	1300	<200
8	<.2	110	n.a.	n.a.	1450	n.a.
9	<.2	190	n.a.	n.a.	1450	n.a.
10	<.2	115	n.a.	n.a.	1300	n.a.
11	<.2	90	n.a.	n.a.	1300	n.a.
12	<.2	100	n.a.	n.a.	1250	n.a.
13	<.2	95	n.a.	n.a.	1300	n.a.
14	<.2	90	n.a.	n.a.	1350	n.a.
15	<.2	105	n.a.	n.a.	1350	n.a.
16	<.2	100	n.a.	n.a.	1250	n.a.
17	<.2	115	n.a.	n.a.	1400	n.a.
18	<.2	115	n.a.	n.a.	1150	n.a.
19	<.2	110	n.a.	n.a.	1250	n.a.
20	<.2	90	n.a.	n.a.	1250	n.a.
21	<.2	100	n.a.	n.a.	1250	n.a.
22	<.2	95	n.a.	n.a.	1200	n.a.
23	<.2	105	n.a.	n.a.	1100	n.a.
24	.2	120	n.a.	n.a.	1050	n.a.
25	<.1	120	93	1300	1400	110
26	<.1	120	95	1300	1400	120
27	<.1	90	85	1300	1300	130
28	<.1	290	93	1400	1700	110
29	<.1	120	91	1300	1500	110
30	<.1	120	86	1400	1400	120
31	<.1	88	90	1400	1400	110
32	<.1	120	86	1300	1300	130
33	<.1	310	90	1300	1400	110
34	<.1	190	95	1300	1400	120
35	.2	175	n.a.	n.a.	1400	n.a.
36	.2	340	n.a.	n.a.	1450	n.a.
37	.2	355	50	2000	1250	<200

Samples 1-6 from unspecified location on sec. 12 outcrop and 7-24 and 35-37 from locations shown on Fig. 2. Analyzed by atomic absorption techniques by Rocky Mountain Geochemical corp. except for Co, Cr, and Zn which were spectrographic analyses by Skyline Labs Inc.

Samples 25-34 are from locations shown on Fig. 2 and analyses are by a semiquantitative spectrographic technique at U.S. Geological Survey analytical laboratories, Reston, Va.

n.a. - not analyzed

Table 5. Comparison of selected trace element contents for average ultramafic rocks and Yellow Dog Plains peridotite (in ppm).

	Turekian & Wedepohl (1961)	Vinogradov (1962)	Goles (1967)	Fisher et al. (1969)*	Wedepohl (1975)	YDP (mean)
Ag	0.06	0.05	--	--	0.05	<0.2 (31)
Cu	10	20	30	41	47	150 (37)
Co	150	200	110	101	110	87 (12)
Cr	1600	2000	2400	3040	3090	1525 (12)
Ni	2000	2000	1500	1581	1450	1350 (37)
Zn	50	30	--	--	56	117 (10)
S**	300	100	--	--	400	1340 (4)

* Data recalculated specifically for 41 peridotites, excluding other ultramafic rock types.

** Sulfur analyses provided by the Institute of Mineral Research, Michigan Technological University.

Note: Parentheses for Yellow Dog Plains (YDP) column enclose numbers of samples analyzed for each element; -- = not given.

TABLE 6.--Summary of data and interpretation of anomalies.
See Figure 6 for location of anomalies

Anomaly	VLF-EM Sign	Ground Magnetics	Gravity	Causitive Feature	Orientation and Extent	Depth Estimate to Top of Body	Remark
An	-	+ 59,900 gammas	Positive anomaly, modelled 30 46 m thick	nearly vertical dike	Generally N 75° W 2.8 km long	Gravity 30-150 m	Probable magnetite mineralization
Bn	-	+ 61,500 gammas	Positive anomaly, modelled 91 m thick	nearly vertical dike	East-West about 800 m long	outcrops	See petrographic analyses
Cn	-	+ 60,000 gammas Complicated magnetics suggest a complexly shaped body	Positive anomaly, modelled 30 m thick	nearly vertical dike	N 80° E 600 m long	outcrops	See petrographic analyses
Ap	+	No apparent expression	Positive anomaly, modelled 15 m thick	nearly vertical dike	N 80° W 1 km long	VLF-EM-37m Gravity-91m	Possible sulfide mineralization
Bp	+	only minor magnetic expression	Positive anomaly, modelled on line 600 W. 61 m thick	Compound swamp, dike, and fault	N 45° W 900 m long	VLF-EM-45m on line 1000 W. Gravity-30m on 600 W	Compound anomaly possible sulfide mineralization
Cp	+	No apparent expression	zero to negative anomaly	Fault zone	N 25° W about 800 m long	None	Geophysics does not indicate sulfide mineralization
Dp	+	No apparent expression	slight positive anomaly, not modelled	Unknown	Irregular generally E-W about 400 m long	None	Nature of causitive body not known but VLF-EM suggests conductivity

Figure I — YELLOW DOG PLAINS
GENERAL REGIONAL GEOLOGY AND LOCATION

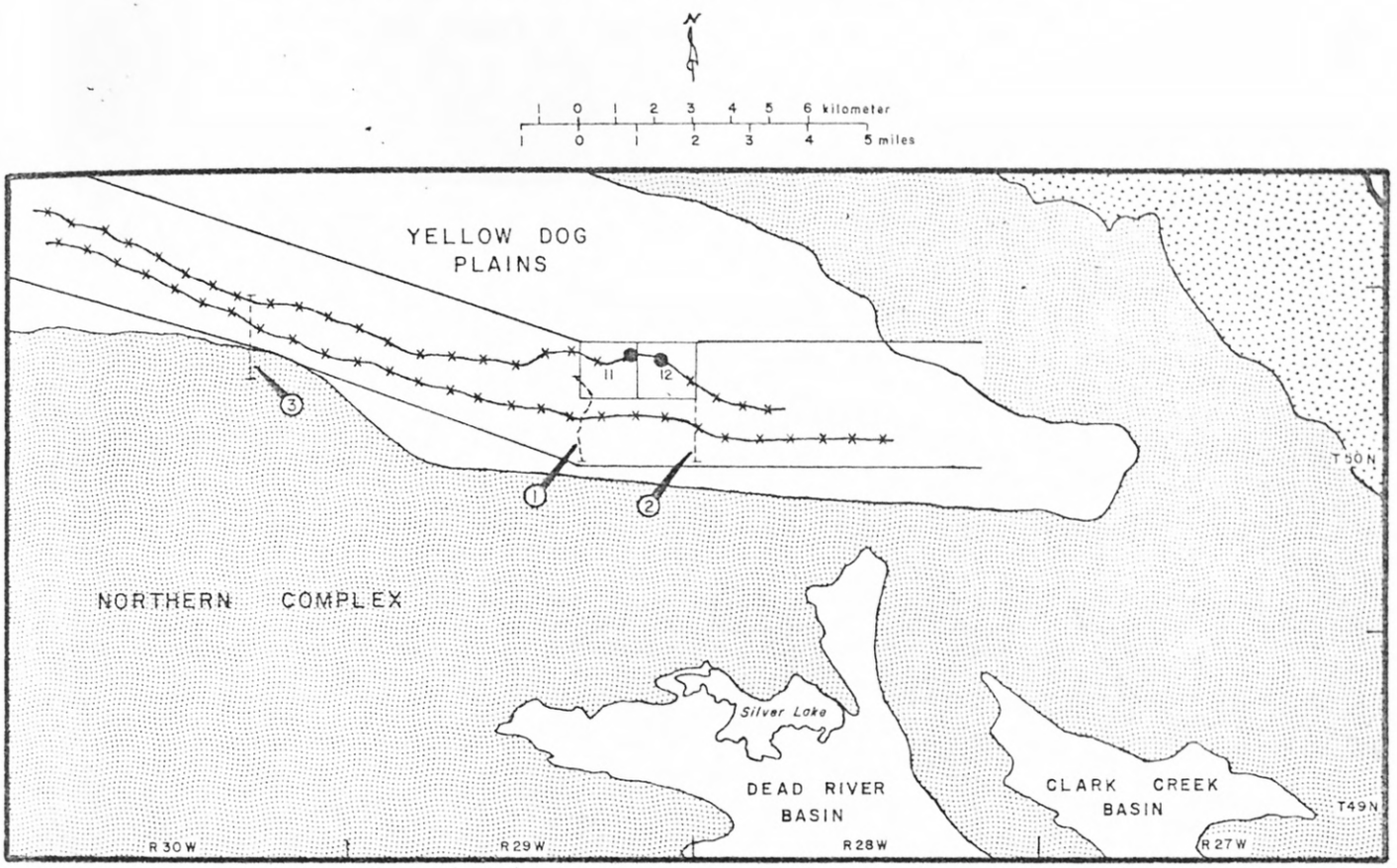

Map base after Case and Gair (1965).

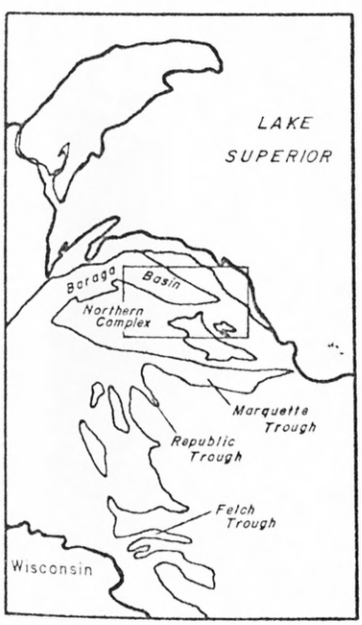

EXPLANATION

① Location of regional geophysical lines

① VLF–EM, gravity, ground magnetics

② gravity, ground magnetics

③ VLF–EM, ground magnetics

Location of two regional aeromagnetic anomalies

General location of outcrops

Location of regional ground magnetic survey

Precambrian Y rocks

Precambrian X rocks

Precambrian W rocks

Figure 2— LOCATION OF ANALYZED SAMPLES

(See figure 3 for exact location of outcrops)

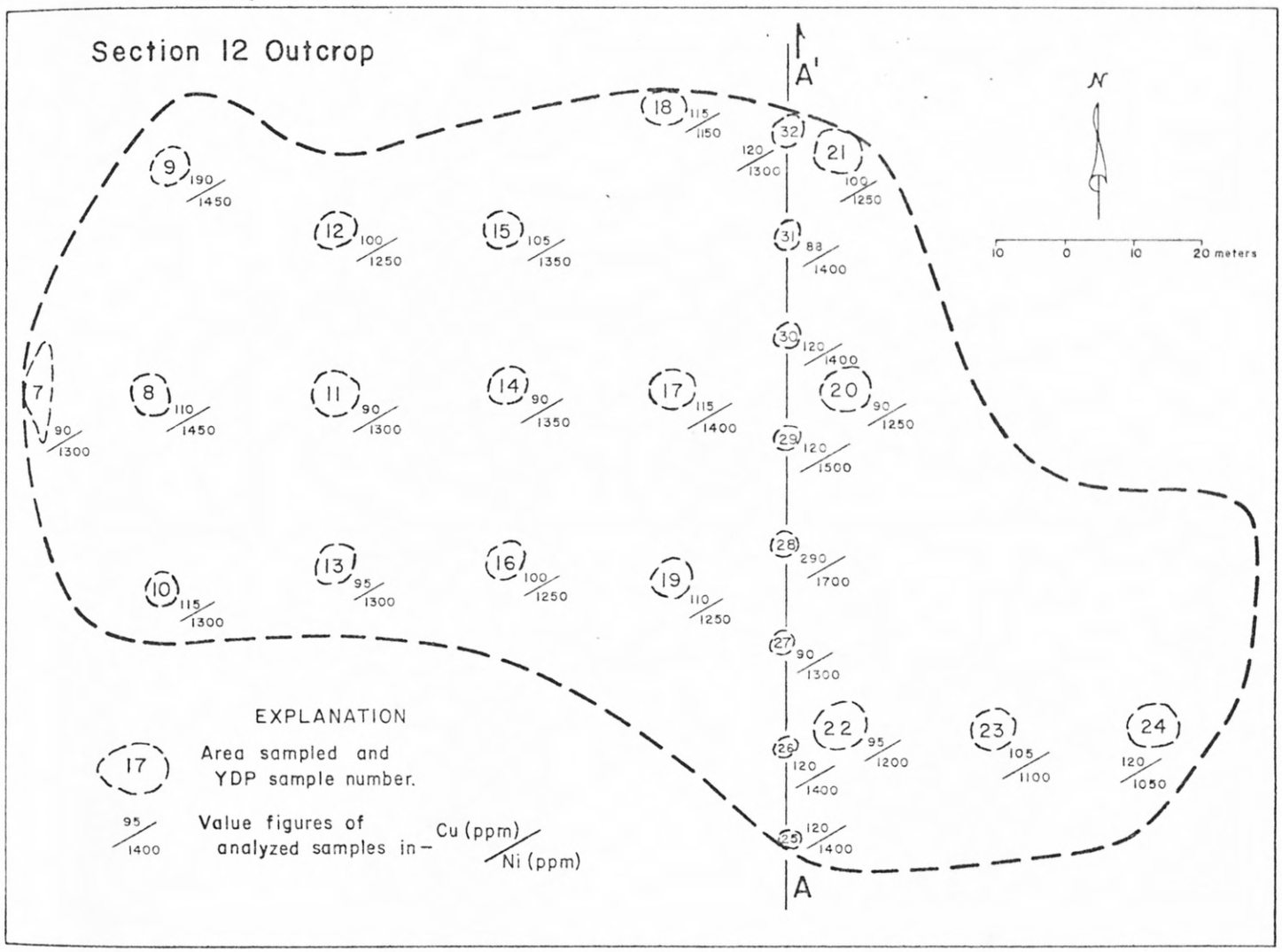

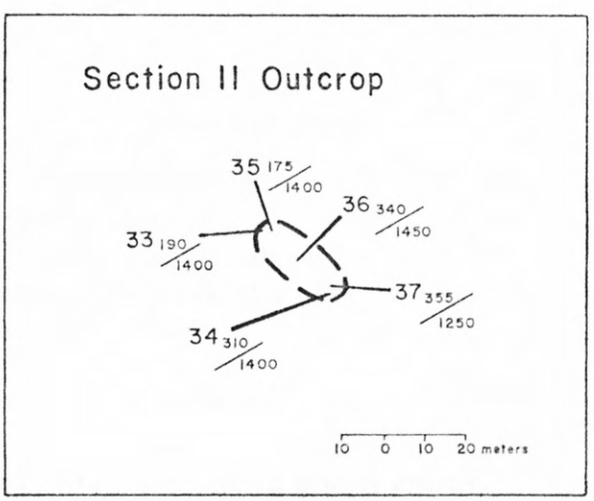

FIGURE 3 — COMPLETE BOUGUER GRAVITY ANOMALY

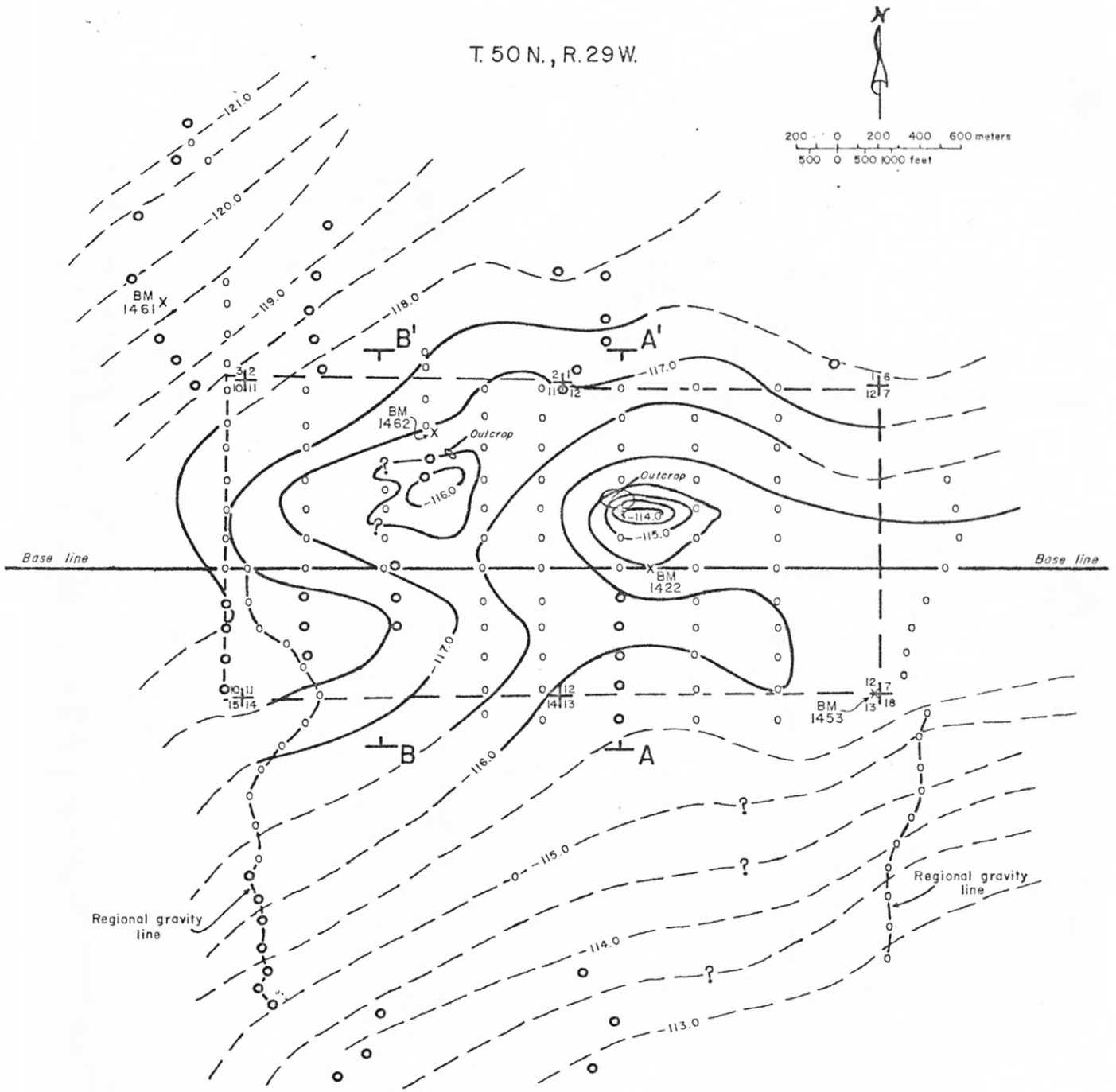

EXPLANATION

Contour interval 0.5 milligals

BM 1422 x — Bench mark

o — Gravity station, elevation surveyed

o — Gravity station, elevation by altimeter

11 12 / 14 13 — Section corner with sections shown

Detailed study area

A' — Position of modeled gravity profile

A

FIGURE 4 – GROUND MAGNETICS OF DETAILED STUDY AREA

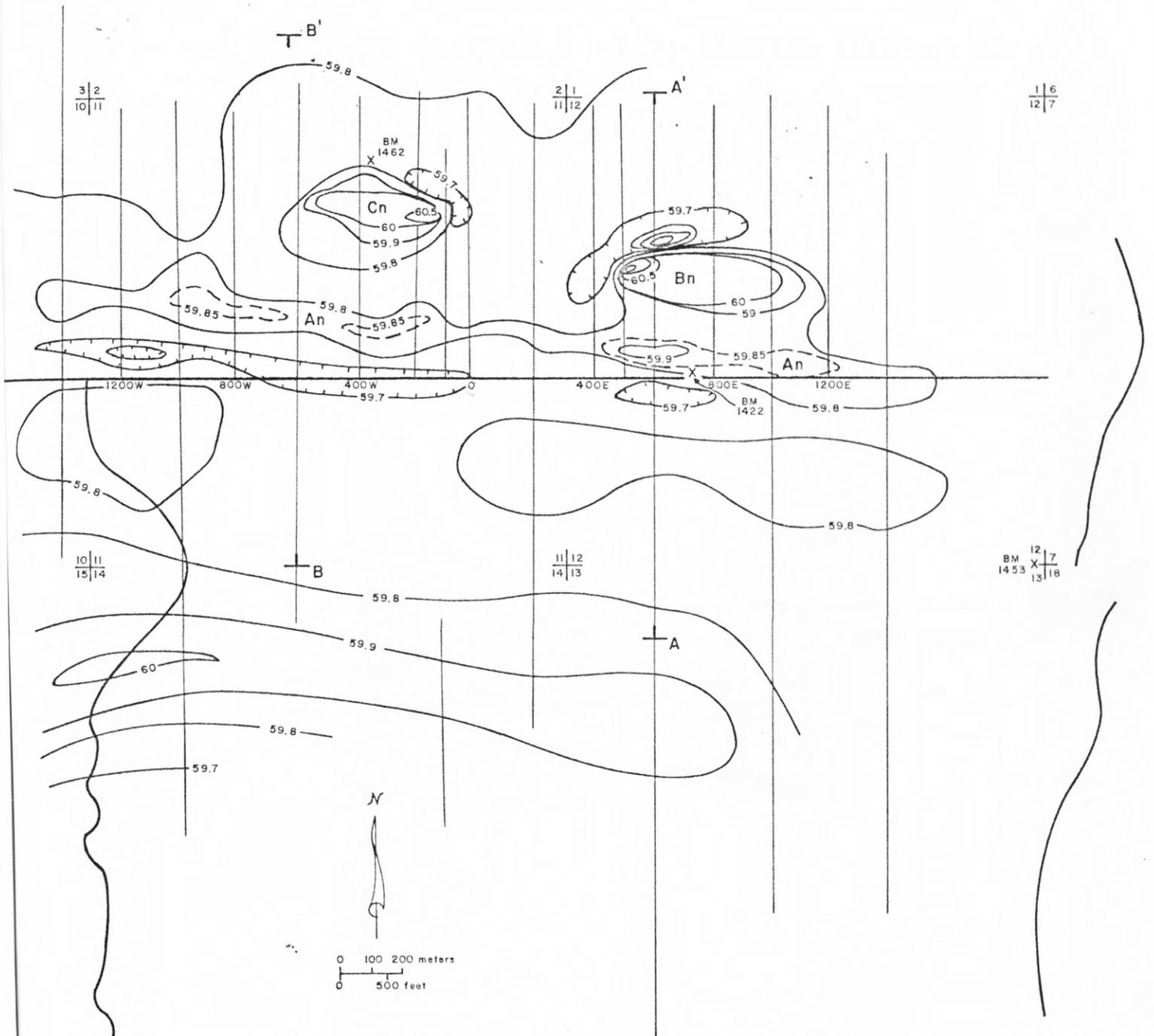

EXPLANATION

Contour interval in thousands of gammas, interval spacing 500 gammas above 60.0 and 100 gammas below 60.0

Extra contour for detail

A' — A Location of modelled profile

Field surveys by: A. Grosz, P. Geraci, R. Lilienthal, D. Snider, 1976

An, Bn, Cn Anomaly designation

FIGURE 5 – DIKES INFERRED FROM GROUND MAGNETICS

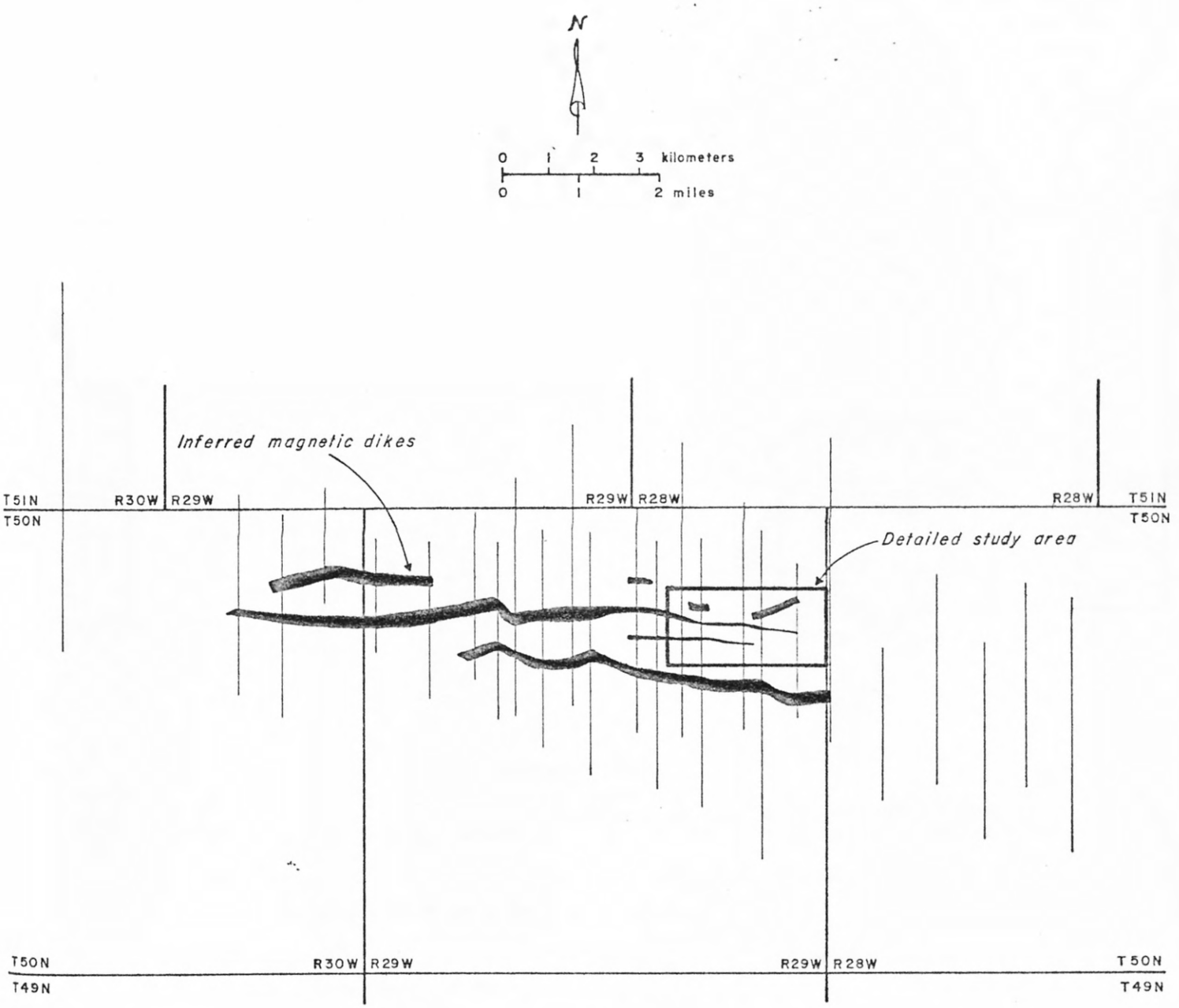

Figure 6 — FILTERED VLF-EM ANOMALIES

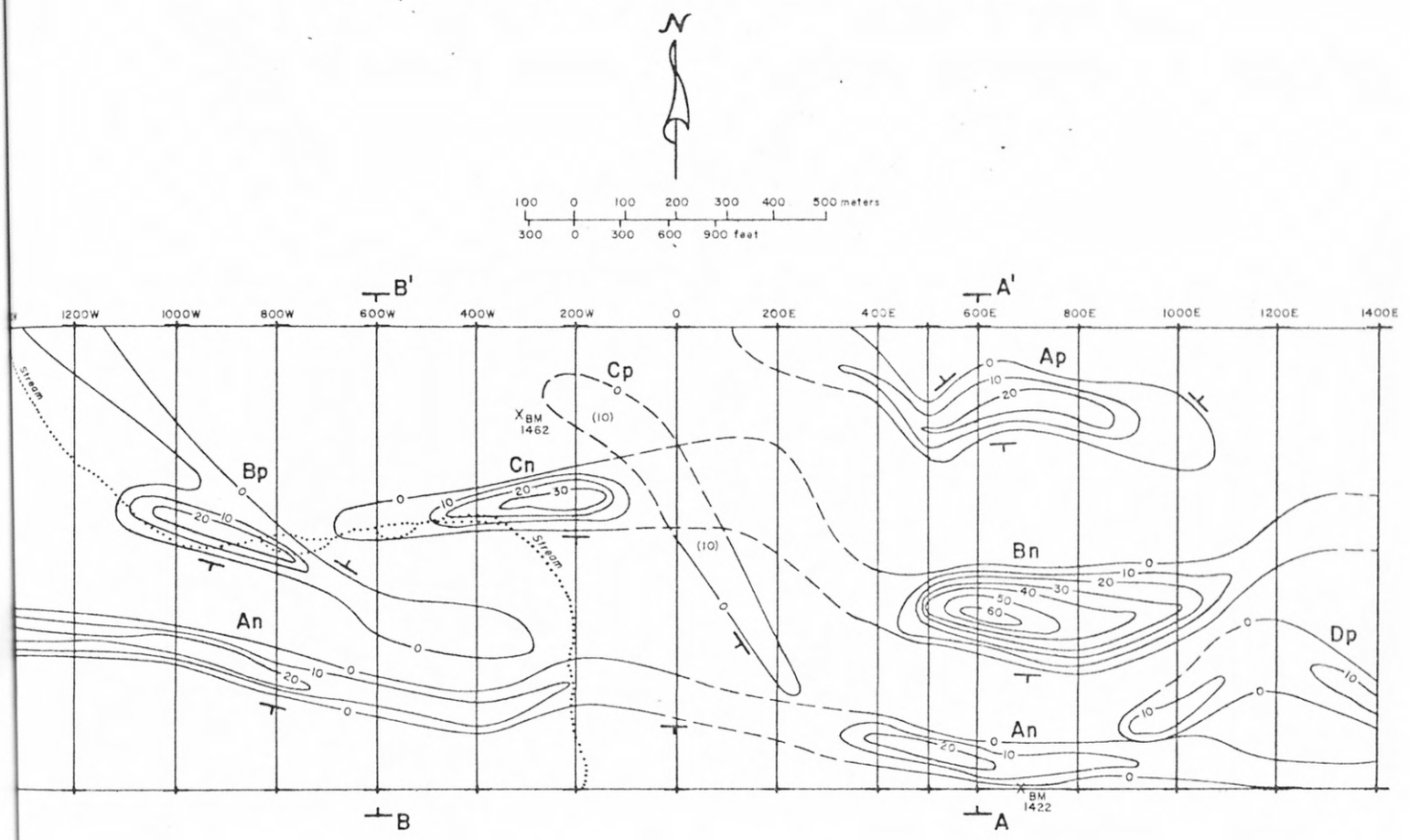

EXPLANATION

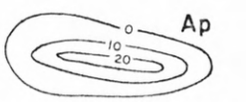

Positive in-phase anomalies.

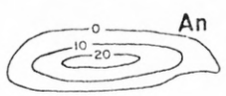

Negative in-phase anomalies.

Indicates line no. and position.

Contour Intervals: 10 Arbitrary filtered units.
Dashed lines are uncertain contours.

Apparent dip direction.

A'
A

Position of modeled profile.

Transmitter Stations

Lines 1400W — 200E
Cutler, Me. 17.8 kHz

Lines 400E — 1400E
Seattle, Wash. 18.6 kHz

FIGURE 7 — GEOLOGY OF THE DETAILED STUDY AREA INFERRED FROM GEOPHYSICAL SURVEYS

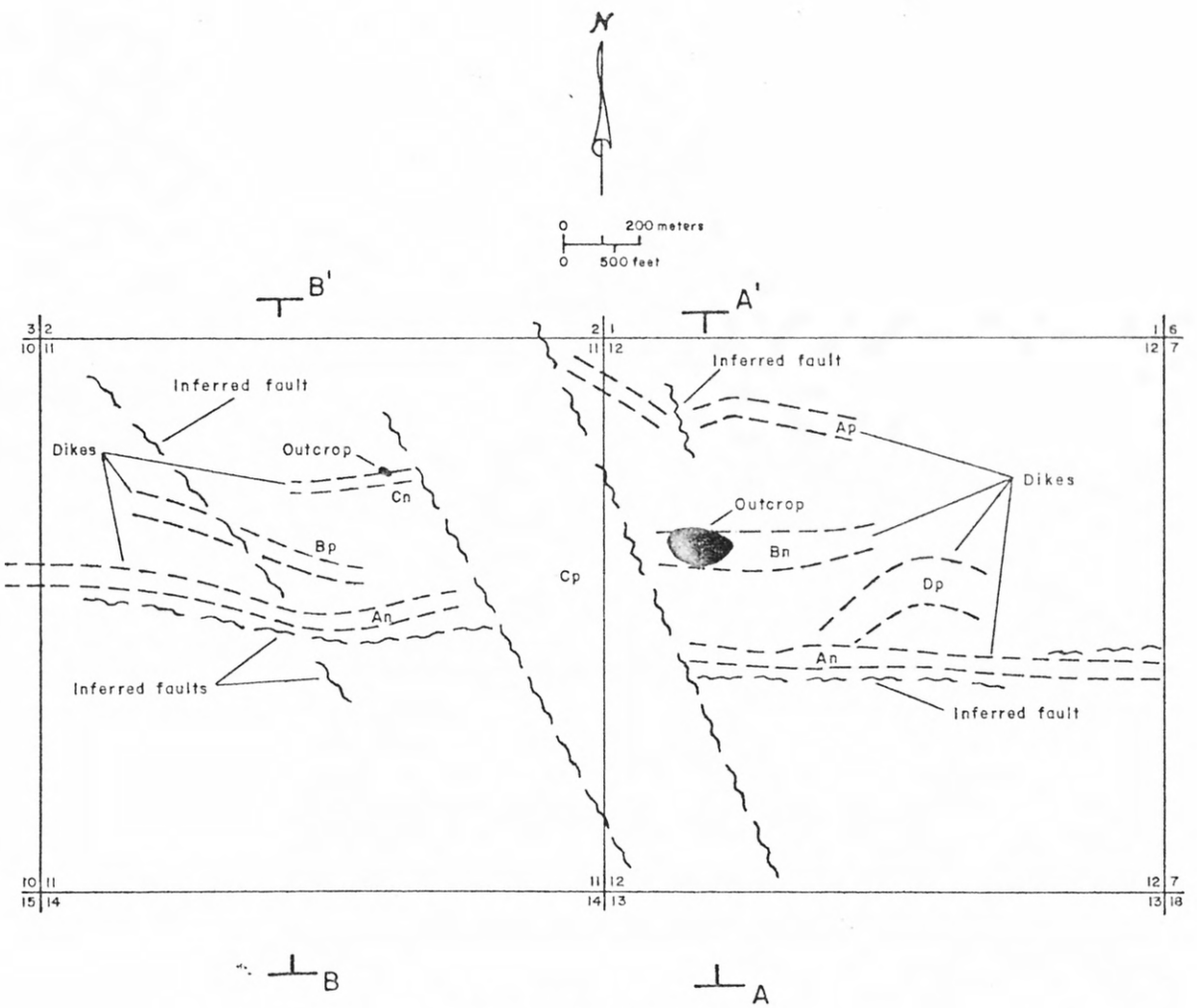

EXPLANATION

A' / A — Location of modelled gravity profile

An, Ap — Letter designating location of geophysical anomaly, with subcript n meaning negative VLF-EM in-phase anomaly and subcript p meaning positive VLF-EM in-phase anomaly.

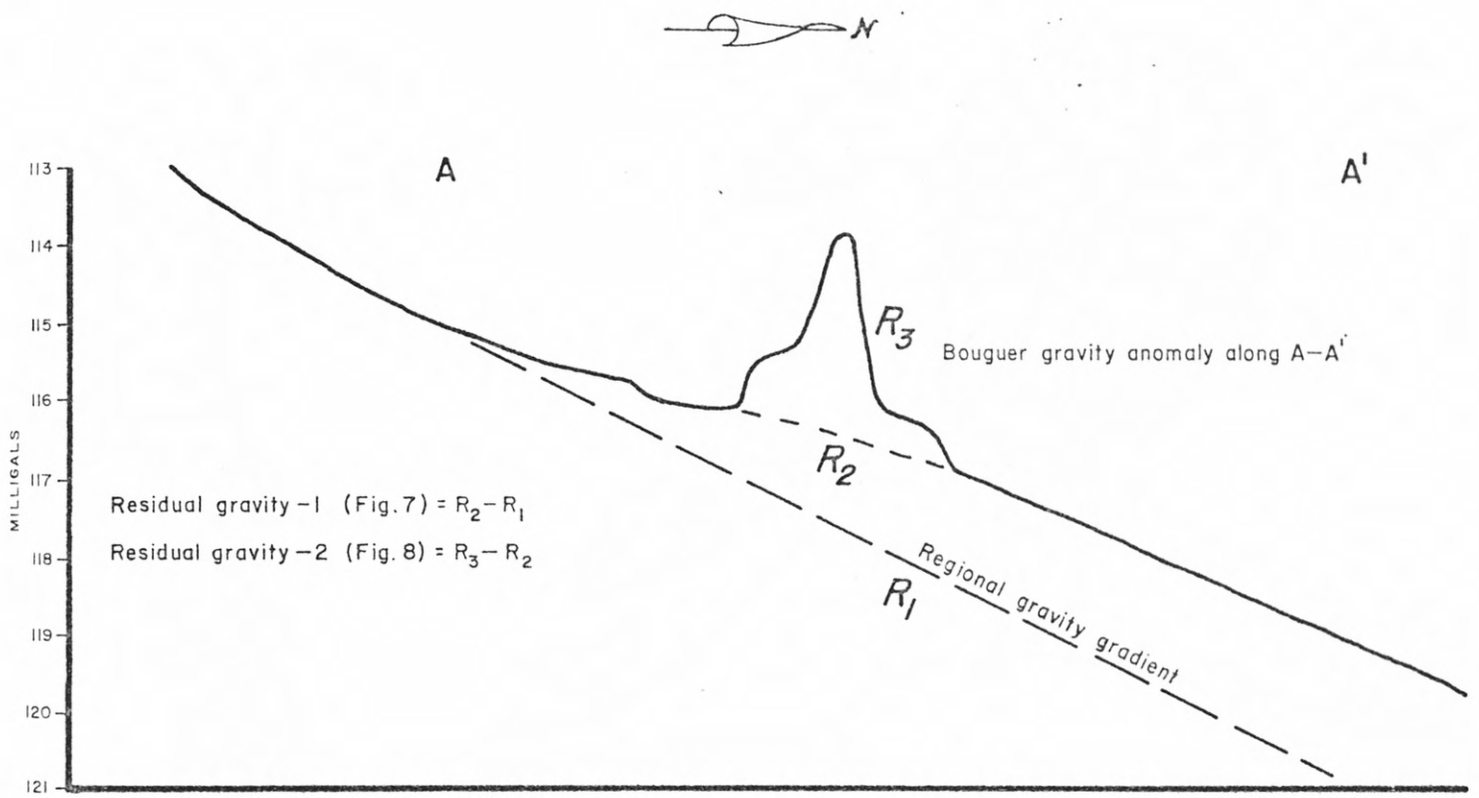

FIGURE 8

GRAVITY PROFILE ALONG A – A'

SHOWING HOW RESIDUAL GRAVITY ANOMALIES WERE DETERMINED

YELLOW DOG PLAINS AREA

FIGURE 9

GRAVITY RESIDUAL - I

(anomaly caused by deep body)

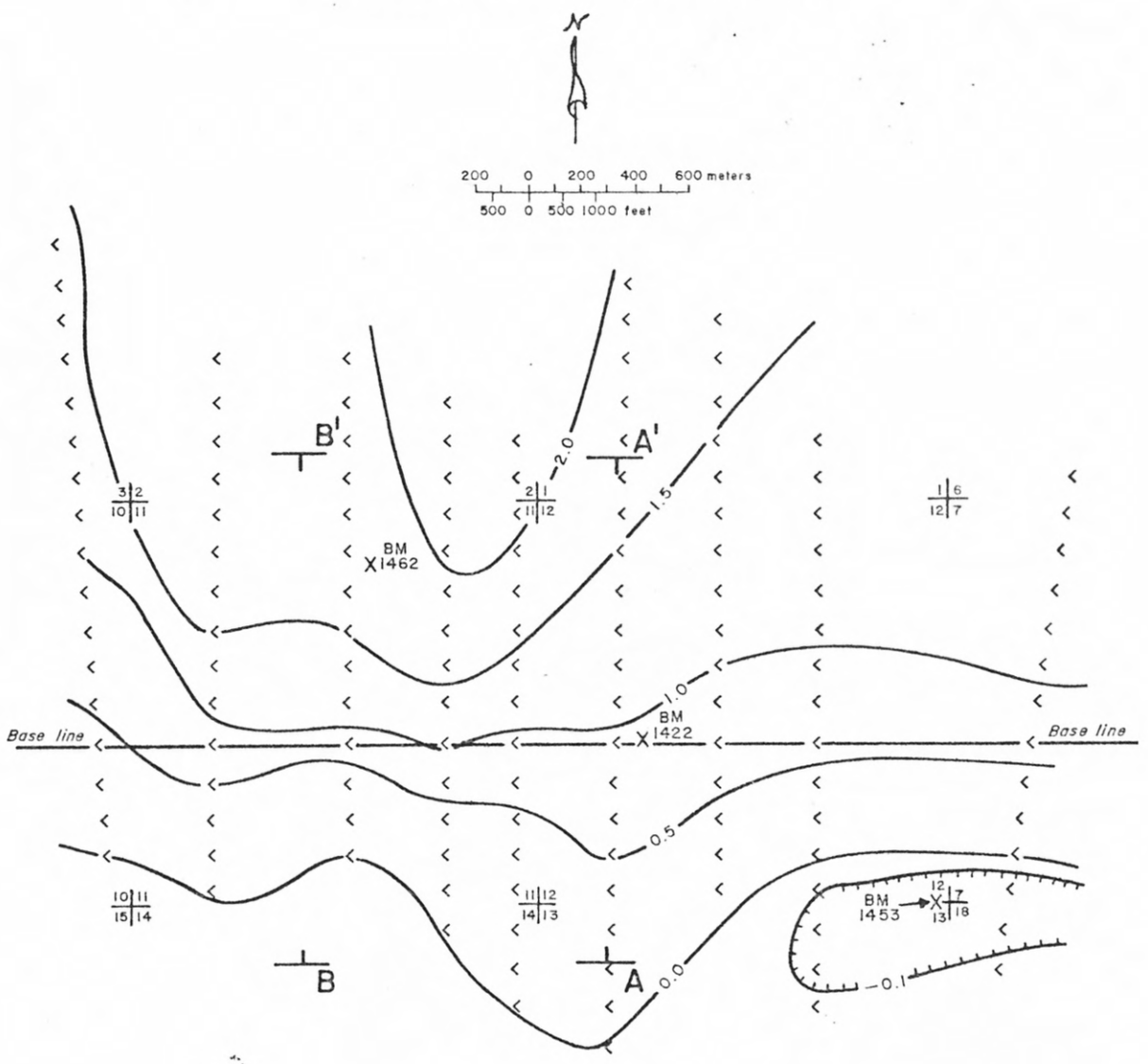

EXPLANATION

Contour interval: 0.5 milligals

< Location of control from graphic analysis

11|12 / 14|13 Section corner with sections shown

X BM 1422 Bench mark

A' Position of modeled gravity profile

A

FIGURE 10

GRAVITY RESIDUAL – 2

(anomaly caused by the near – surface dikes)

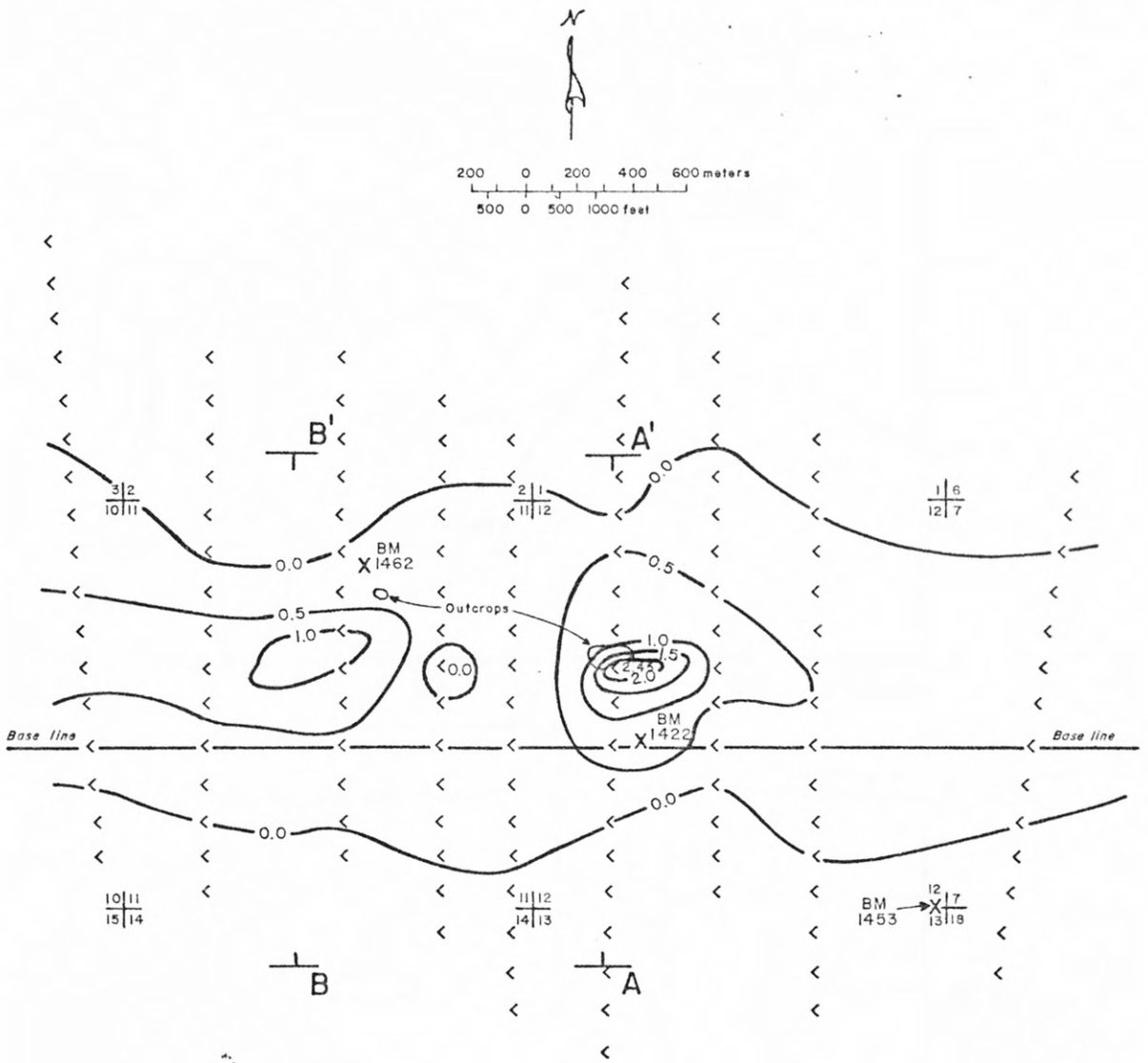

EXPLANATION

Contour interval: 0.5 milligals

< Location of control from graphic analysis

11|12 / 14|13 Section corner with sections shown

X BM 1422 Bench mark

A' Position of modeled gravity profile

A

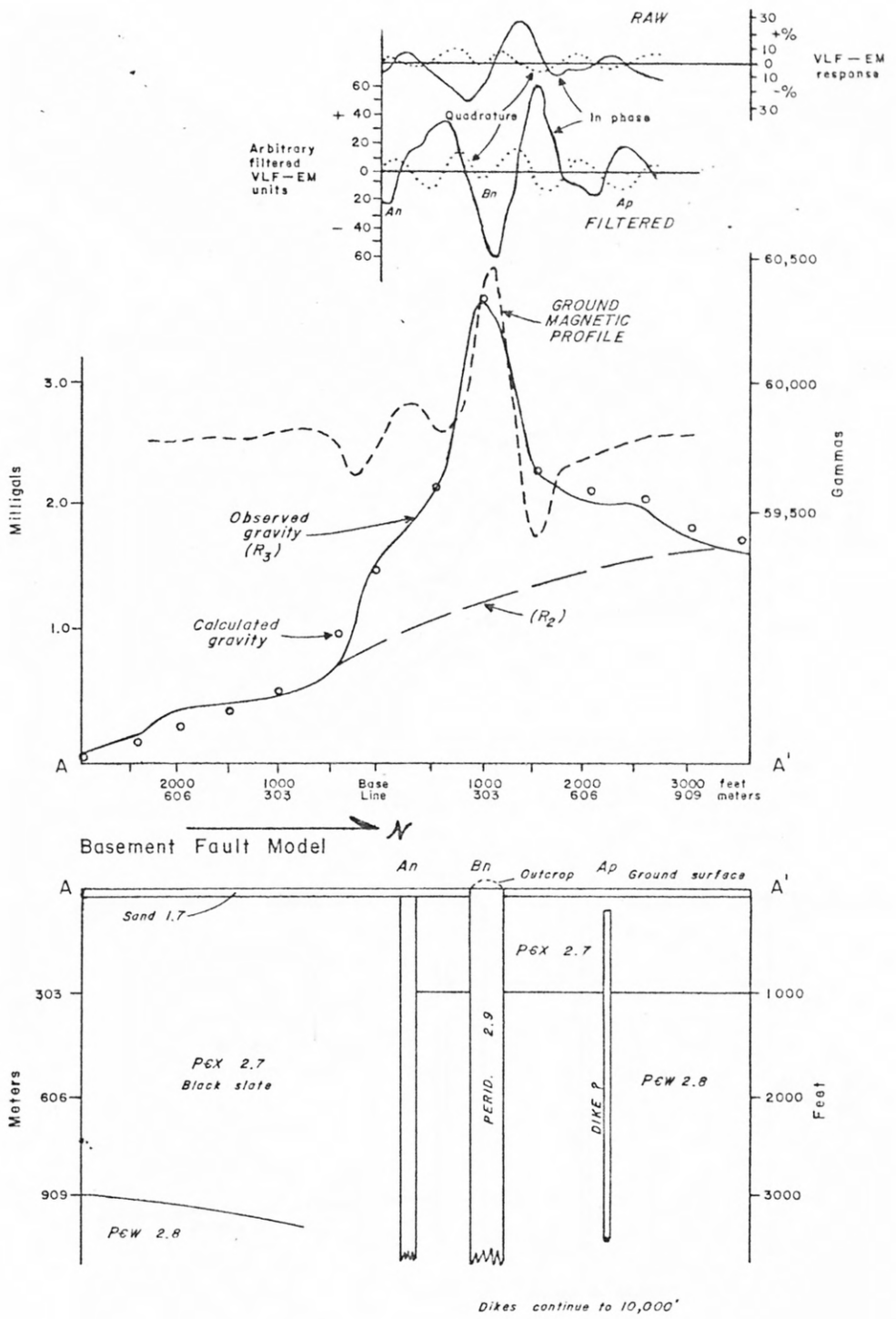

FIGURE IIA

COMPOSITE GEOPHYSICAL PROFILES AND GEOLOGIC MODEL FOR CROSS-SECTION A-A'

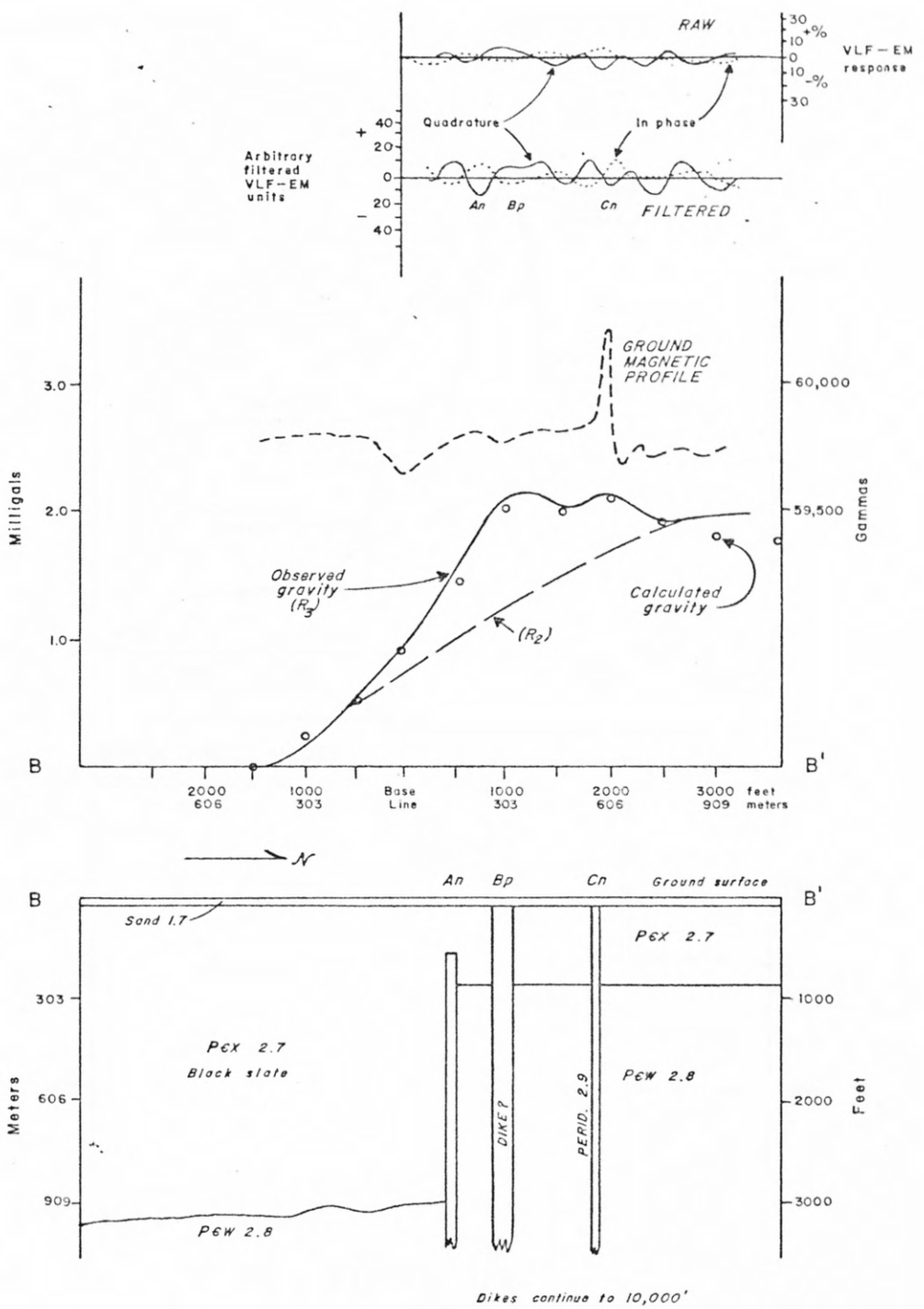

FIGURE 11 A (cont.)

COMPOSITE GEOPHYSICAL PROFILES AND GEOLOGIC MODEL FOR CROSS-SECTION B–B'

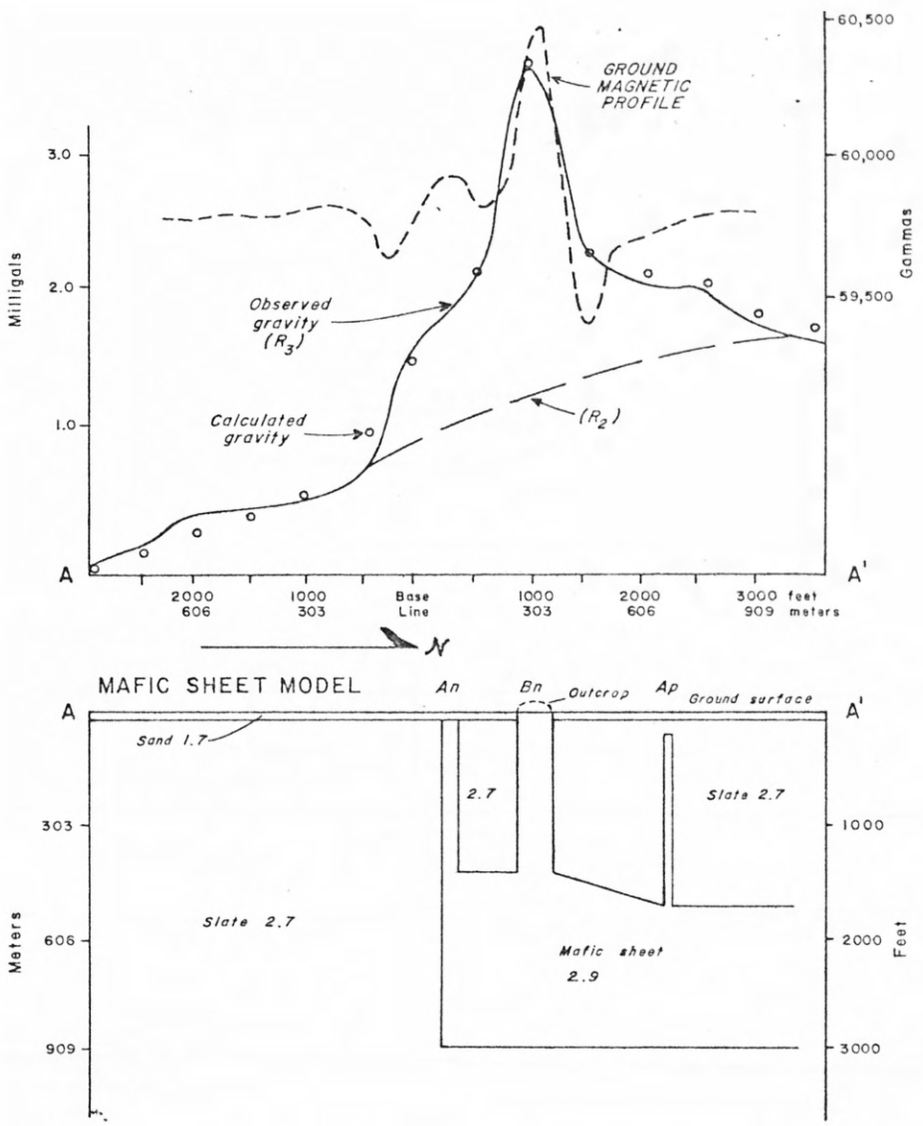

FIGURE IIB

COMPOSITE GEOPHYSICAL PROFILES AND ALTERNATE GEOLOGIC MODEL (MAFIC SHEET) FOR CROSS-SECTION A–A'

FIGURE 12 — COMPOSITE GEOPHYSICAL PROFILES ALONG REGIONAL LINES 1 AND 3

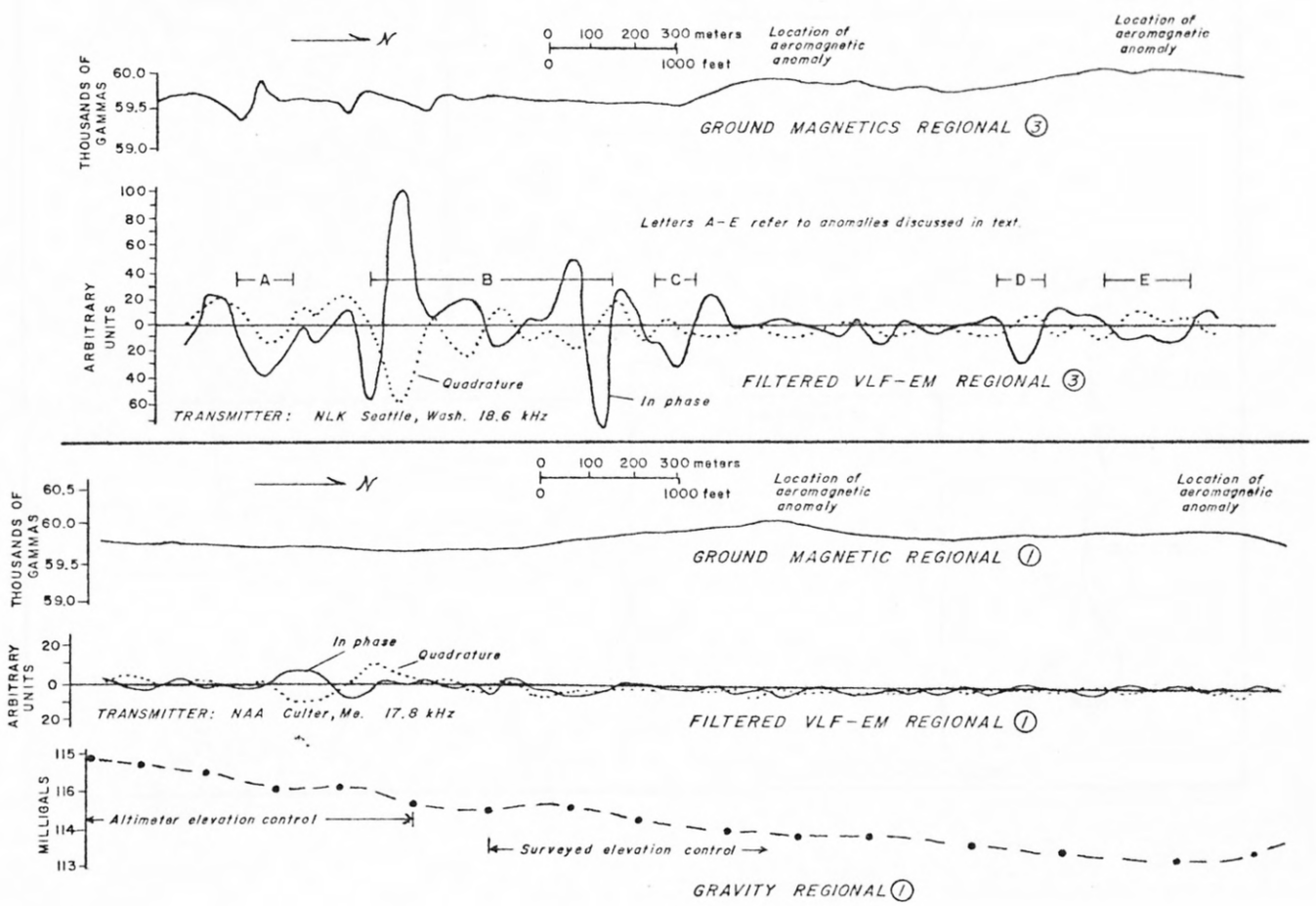

FIGURE 13 — LOCATION OF GEOCHEMICAL SOIL PROFILES

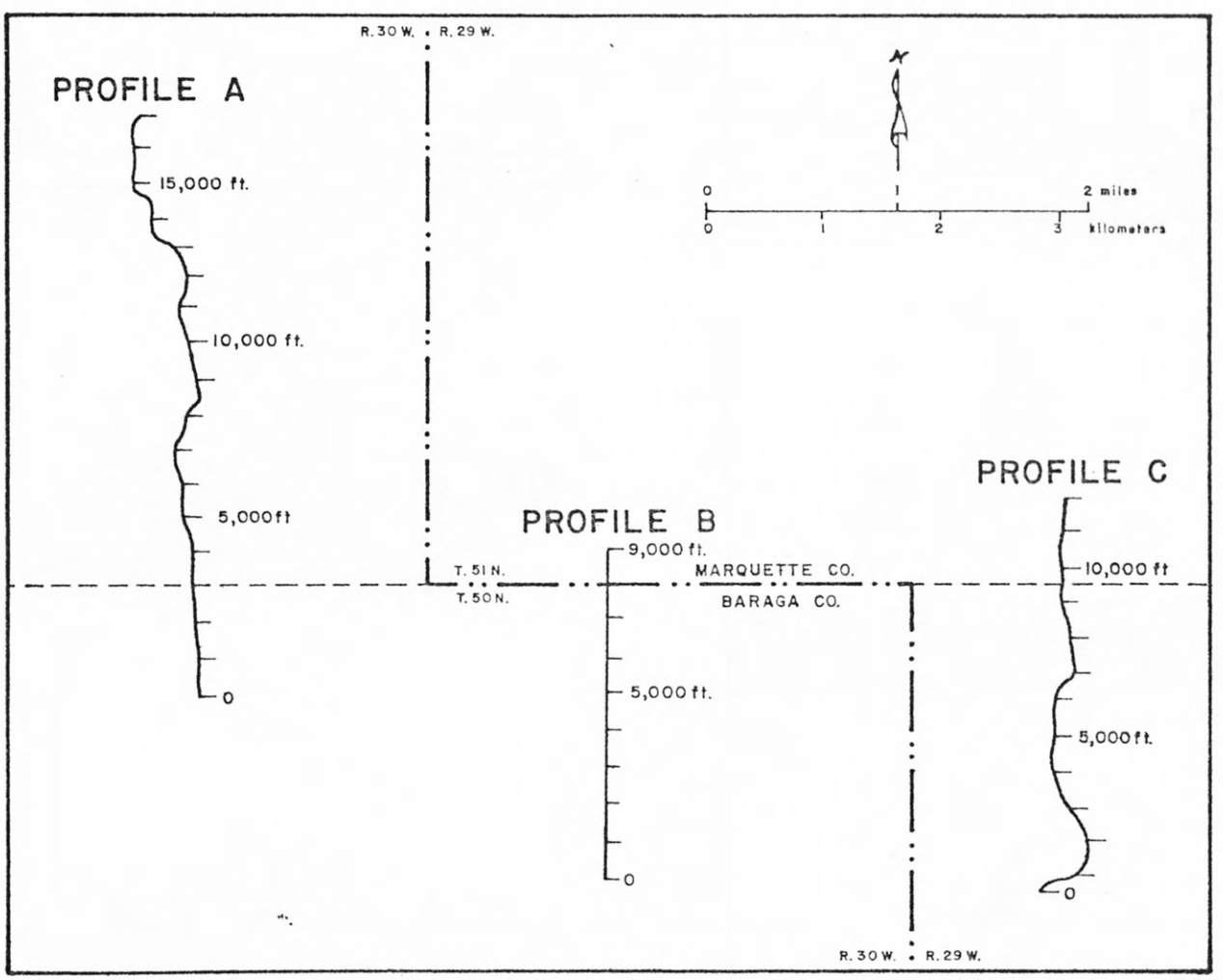

FIGURE 14 — GEOCHEMICAL PROFILES IN SOIL ALONG PROFILE A

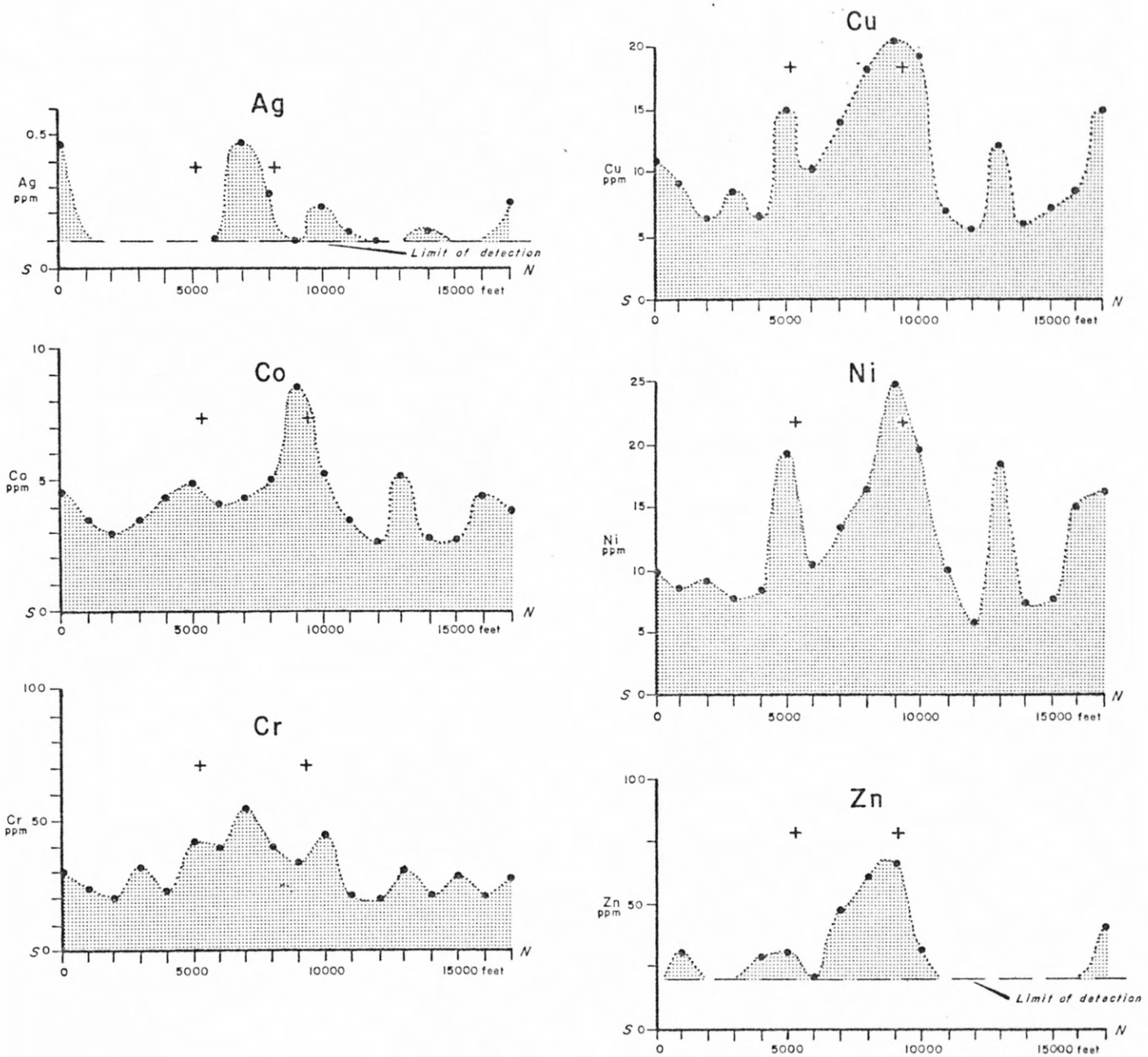

\+ Crest of aeromagnetic anomaly

FIGURE 15 – GEOCHEMICAL PROFILES IN SOIL ALONG PROFILE B

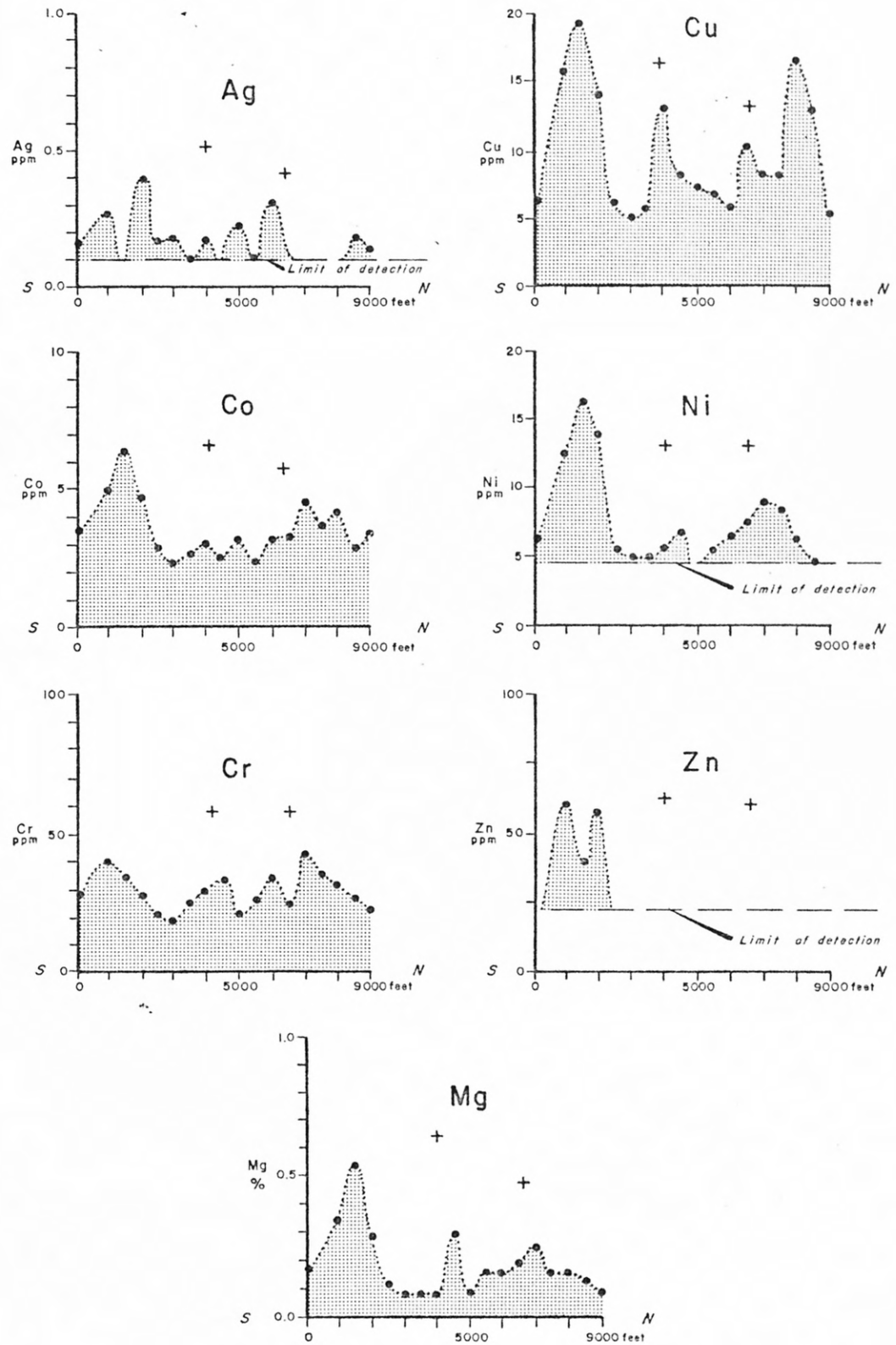

\+ Crest of aeromagnetic anomaly